STUDIES OF PLATELET GPIB-ALPHA AND VON WILLEBRAND FACTOR BOND FORMATION UNDER FLOW

A Dissertation
Presented to
The Academic Faculty

by

Leslie Ann Coburn

In Partial Fulfillment
of the Requirements for the Degree
Doctor of Philosophy in the
School of Biomedical Engineering

Georgia Institute of Technology and Emory University
May 2010

STUDIES OF PLATELET GPIB-ALPHA AND VON WILLEBRAND FACTOR BOND FORMATION UNDER FLOW

Approved by:

Dr. Larry V. McIntire, Advisor
Wallace H. Coulter Department of
Biomedical Engineering
Georgia Institute of Technology
and Emory University School of Medicine

Dr. Miguel Cruz
Department of Medicine
Thrombosis Research Section
Baylor College of Medicine

Dr. Suzanne G. Eskin
Wallace H. Coulter Department of
Biomedical Engineering
Georgia Institute of Technology
and Emory University School of Medicine

Dr. Elliot Chaikof
Wallace H. Coulter Department of
Biomedical Engineering
Georgia Institute of Technology
and Emory University School of Medicine
Department of Surgery
Emory University School of Medicine

Dr. Cheng Zhu
Wallace H. Coulter Department of
Biomedical Engineering
Georgia Institute of Technology
and Emory University School of Medicine

Date Approved: March 8, 2010

To my family and friends, who inspire me daily

ACKNOWLEDGMENTS

I would like to express my deep gratitude to all those involved in my journey completing this dissertation and my graduate studies. First, I would like to thank my advisors Dr. Larry V. McIntire and Dr. Suzanne G. Eskin for their tireless support, help in innumerable areas of my research and career pursuits, and guidance throughout my graduate studies. I also appreciate the support and guidance of the rest of my thesis committee members: Dr. Cheng Zhu, Dr. Miguel Cruz, and Dr. Elliot Chaikof. I would like to thank Dr. Cheng Zhu for his guidance on catch bonds and frame-by-frame analysis of rolling interactions. I would like to thank Dr. Miguel Cruz for providing all vWF-A1 and vWF-A1A2A3 molecules, which were essential to my research.

I would like to thank Dr. Rodger McEver for graciously allowing me to visit his lab for an extended period of time to learn how rolling interactions were observed, recorded, and analyzed. Further, I would like to thank McEver lab members Dr. Tadayuki Yago and Jonathan Miner for taking time out of their already-full days while I was visiting to instruct me in the details of how the McEver lab gathers and analyzes rolling interaction data.

I would like to thank the current and former members of the McIntire lab. In particular, I would like to thank Dr. Marcie Williams for her assistance in understanding rolling interactions and flow chamber assays. Further, I would like to thank two outstanding undergraduates that I had the pleasure of mentoring during my studies,

Sejdefa Dozic and Venkata Damaraju, whose work provided valuable information furthering my research.

Lastly, I would like to express my deep gratitude to my family and friends. In particular, I would like to thank my mom, Beneta Williams, whose constant support and unwavering encouragement give me guidance and direction to pursue my dreams. I would also like to thank Archana Chawda for her friendship and support. Finally, I would like to thank Christopher Henke for his support, encouragement, and friendship, and also for his computer programming expertise.

TABLE OF CONTENTS

LIST OF TABLES

LIST OF FIGURES

LIST OF ABBREVIATIONS

A	Constant determined from Table I (a = R, h = h) in [1]
ADAMTS-13	A disintegrin and metalloproteinase with a thrombospondin type 1 motif, member 13
AFM	Atomic force microscopy
CHO	Chinese hamster ovary
E. coli	Escherichia coli
FITC	Fluorescein isothiocynate
FRET	Fluorescence resonance energy transfer
F_S	Shear force
GOF	Gain-of-function
GPIbα	Glycoprotein Ibα
h	Distance from the center of the cell to the wall
HRP	Horseradish peroxidase
HSA	Human serum albumin
k_{off}	Off-rate
LOF	Loss-of-function
N_b	Number of cells tethered
PSGL-1	P-selectin glycoprotein ligand - 1
pt-VWD	Platelet type von Willebrand Disease
R	Cell diameter

RGD	Arginine-Glycine-Aspartic Acid
RIPA	Ristocetin induced platelet aggregation
RPE	R- Phycoerythrin
TTP	Thrombotic thrombocytopenic purpura
VWD	von Willebrand disease
vWF	von Willebrand factor
wt	Wild type
γ	Shear rate
μ	Viscosity

SUMMARY

Understanding the differential bonding mechanics underlying bleeding disorders is of crucial importance to human health. In this research insight is provided into how four of these bleeding disorders (each with somewhat similar clinical characteristics), work at the molecular bond level. The bleeding diseases studied here can result from defects in the platelet glycoprotein (GP) Ibα, the von Willebrand factor (vWF) molecule, or the ADAMTS-13 enzyme. Types 2B and 2M von Willebrand Disease (VWD) result in excess bleeding, yet type 2B has increased binding affinity between platelet GPIbα and vWF, while type 2M has decreased binding affinity between these two molecules. Platelet type VWD (pt-VWD) causes mutations in the GPIbα molecule and has similar characteristics to type 2B VWD. Further, in thrombotic thrombocytopenic purpura, bleeding results when there is a lack of active ADAMTS-13 enzyme. Each disease results in patient bleeding, but due to different mechanisms. This dissertation will explore the bonding mechanics between GPIbα and vWF and how they are altered in each disease state. To observe the GPIbα-vWF bonding mechanics, rolling velocities, transient tethering lifetimes, and tether frequency were determined using a parallel plate flow chamber. Data from these experiments suggest that wt-wt interactions are force dependent and have biphasic catch-slip bonding behavior. The data show that the shear stress at which the maximum mean stop time occurs differs between gain-of-function and loss-of-function mutations. Using similar methods, we study the changes resulting from pt-VWD mutations in GPIbα, and find that the catch bond seen for wt-wt interactions is lost for these mutations. Further, the data suggest that interactions with gain-of-function

GPIbα mutations may be transport rather than force dependent. Finally, how the GPIbα-vWF tether bond changes for thrombotic thrombocytopenic purpura was also investigated to show that the bond lifetime in the absence of the enzyme is increased presenting a possible rationale for why bleeding occurs in this disease. Overall, the data show how the bonding mechanics of the GPIbα-vWF tether bond differ in four bleeding diseases. Further, these observations offer potential explanations for how these changes in the bonding mechanism may play a role in the observed patient bleeding.

CHAPTER 1: THESIS RATIONALE AND SPECIFIC AIMS

1.1 Thesis Rationale

Activated platelets mediate the homeostatic response to vascular injuries. In arteries, this response is initiated specifically by platelet receptor glycoprotein (GP) Ibα tethering to von Willebrand factor (vWF) on exposed subendothelium. Platelet GPIbα interacts with vWF to initiate rolling interactions that are the first step in the formation of a hemostatic plug at a site of vascular injury. Following this initial step, platelets activate, firmly adhere via the GPIIb/IIIa integrin, and aggregate to form the plug and stop bleeding [2]. Mutations in either vWF or GPIbα can disrupt this step in hemostasis resulting in the bleeding disorders von Willebrand disease (VWD) or platelet type von Willebrand disease (pt-VWD), respectively [3]. Disruption of the normal interactions between these molecules can also lead to thrombosis as seen in thrombotic thrombocytopenic purpura [4].

Evidence suggests that mutations in either vWF or GPIbα may lead to abnormal interactions between platelet GPIbα and soluble vWF. In Type 2B VWD it is believed that increased aggregation of platelets with soluble vWF leads to bleeding due to clearance of these aggregates, which results in a lack of unbound GPIbα receptors to interact at sites of vascular injury [5].

VWD type 2M loss-of-function (LOF) mutations in vWF or Bernard Soulier Syndrome causing mutations in platelet GPIbα show decreased binding affinity resulting in increased rolling velocities and off-rates. These types of mutations are characterized

by defective ristocetin binding and normal botrocetin binding. Type 2M VWD mutant G561S shows decreased ristocetin binding and normal multimer number, formation and pattern [6]. It is thought that these mutations result in a defect that prevents the vWF molecule from undergoing a conformational change that prevents normal binding to GPIbα [7].

Mutations in the GPIbα molecule have been observed that lead to patient bleeding. The binding of these mutations has been shown to be similar to that seen in type 2B VWD and is characterized by increased association between GPIbα and vWF [8].

The overall goal of this research was to investigate both the interactions for wt-wt platelet-vWF interactions, as well as for wt-mutant or mutant-wt platelet-vWF interactions. Parallel plate flow chamber experiments were used to mimic physiological flow conditions and were conducted at 37^{o}C and interactions were recorded at 250 fps. One gain-of-function (GOF) mutation was selected for mutations in platelet GPIbα (K237V). One GOF and one LOF mutation were chosen to represent changes in the vWF-A1 domain (R687E and G561S, respectively). Rolling velocities, mean stop times, mean go times, and transient tethering lifetimes were determined to give insight into GPIbα-vWF interactions.

1.2 Specific Aims

1.2.1 Specific Aim I: To Investigate the Rolling Interactions of the Wild-Type GPIbα-vWF Tether Bond Under Low Shear Forces.

Here it is hypothesized that platelet GPIbα and vWF-A1 interact via a catch bond mechanism under normal physiological conditions. To determine if a catch bond was present platelet-vWF interactions were studied to observe trends in several parameters. First, rolling velocities were measured for platelets or CHO cells expressing GPIbα rolling on vWF molecules. The trend observed for these interactions indicates the type of bond that may be present between these two molecules. If the velocity decreases with increasing shear stress, the data suggest that most likely the bond lifetime is increased as the shear stress is increased. However, if the velocity increases with increasing shear stress, the data suggests that the bond lifetime is decreasing with increasing shear stress. Increasing bond lifetime with increasing shear stress is suggestive of a region of catch bond behavior, while decreasing bond lifetime with increasing shear stress is suggestive of a region of slip bond behavior. To further study rolling interaction and bond lifetimes, the mean stop time of the interactions was determined. Mean stop time, which suggests information about the bond lifetime, can be used as an indicator for the off-rate of the bond, which is inversely proportional to the bond lifetime. If the mean stop time increases with increasing shear stress, it is likely that the bond lifetime is increased. This result in turn implies that the off-rate for the bond is decreasing with increasing shear stress, suggesting that a catch bond is present. Inversely, if the mean stop time is decreasing with increasing shear stress, then the bond lifetime is decreasing and the off-rate is increasing with increasing shear stress, suggesting the presence of a slip bond.

Because the bond lifetime may be controlled by either transport or force dependent mechanisms, next the rolling velocities and mean stop times were determined while changing the viscosity at a given shear rate. If the experiments are done in medium

of increased viscosity, and data align when plotted against shear stress, then the data suggests that the interactions are force dependent. While, if the data align when plotted against shear rate, then the data suggest that the interactions are force independent and transport dependent. Because on-rate changes result from transport mechanisms and off-rate changes result from force mechanisms, it is likely that if the interactions are force dependent, then the off-rate would be a controlling parameter and, vice versa, that if the interactions are transport dependent, then the on-rate would be a controlling parameter for platelet-vWF rolling interactions.

1.2.2 Specific Aim II: To Investigate the Effects of Mutations in the vWF-A1 Binding Site on the Biomechanics and Kinetics of Bond Formation and Dissociation.

Here it is hypothesized that mutations in the vWF-A1 domain result in different binding properties between platelet GPIbα and vWF molecules. It is also hypothesized that GOF mutations in the vWF-A1 domain result in the loss of a catch bond at lower shear stresses under physiological conditions. Loss of the catch bond could explain how increased aggregation of platelets with soluble vWF in type 2B VWD leads to bleeding due to clearance of these aggregates or due to a lack of unbound GPIbα receptors to interact at sites of vascular injury. Further, it is hypothesized that LOF mutations in the vWF-A1 domain interact with platelets via a catch bond mechanism under physiological conditions, but that the catch-slip transition is shifted to higher shear stress. This shift could result in a decreased likelihood that platelet binding will occur under shear stress

conditions where the molecule is stabilized because at these higher shear stresses, the flow is too great to allow for enough cells to be near the surface long enough to bind.

To study changes due to VWD states, the GOF mutation R687E and LOF mutation G561S were studied in the isolated vWF-A1 domain and compared to results seen for wt vWF molecules. Interactions between platelets and mutant vWF-A1 domains were studied by measuring rolling velocities, mean stop times, and transient tethering lifetimes, and were analyzed using the same methods that were used for wt-wt interactions.

1.2.3 Specific Aim III: To Investigate The Effects Of Mutations In the Platelet GPIbα Binding Site On the Biomechanics and Kinetics of Bond Formation and Dissociation.

Here it is hypothesized that mutations in the GPIbα molecule result in different binding between platelet GPIbα and vWF-A1 and that GOF mutations in the GPIbα molecule result in the loss of a catch bond at lower shear stresses under physiological conditions. Platelet type VWD is characterized similarly to type 2B VWD, where mutations result in bleeding due to increased interactions between GPIbα and vWF. It is believed that the mutations in the GPIbα molecule result in bulk aggregation and clearance of platelets. As with the type 2B VWD mutations, a loss of the catch bond could explain increased aggregation between these molecules.

To study changes due to pt-VWD states, the GPIbα GOF mutation K237V was expressed on CHO cells and compared to results seen for wt GPIbα molecules expressed on CHO cells and platelets. Interactions between CHO cells expressing GPIbα (wt or

mutant) and the wt vWF-A1 domain were studied by measuring rolling velocities, mean stop times, and transient tethering lifetimes, and were analyzed using the same methods as described in Specific Aim I.

CHAPTER 2: BACKGROUND AND SIGNIFICANCE

2.1 Thrombosis and Hemostasis and Normal Physiological GPIbα-vWF Interactions at the Vessel Wall

As described in Chapter 1, activated platelets mediate the homeostatic response to vascular injuries. Normally, interactions between platelet GPIbα and vWF are the first interactions in response to a vascular injury. When vascular injury occurs, vWF located in the subendothelial matrix becomes exposed. The GPIbα receptor located on platelets then can interact with the exposed vWF molecule. In order for rapidly flowing platelets to interact with the vWF at the stationary wall, they must first be slowed down.

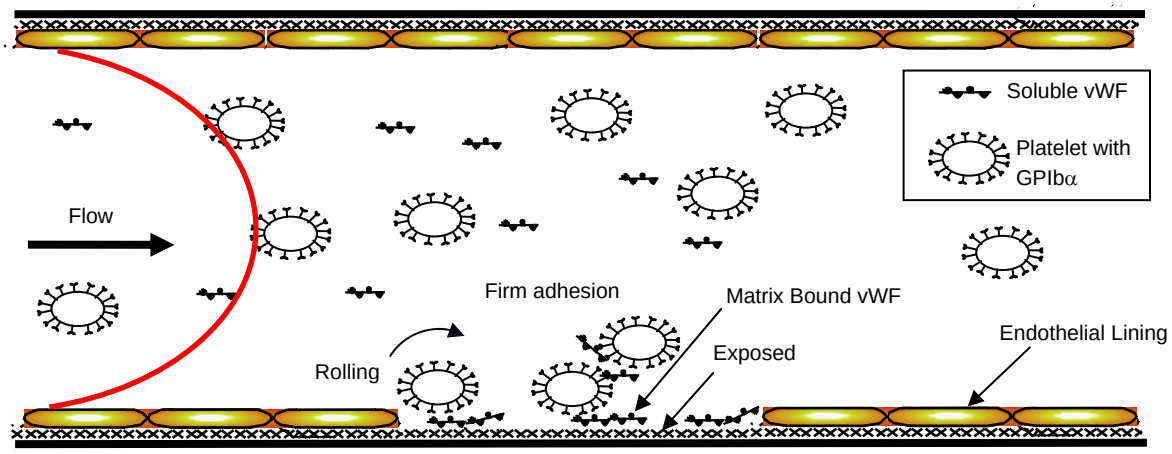

Figure 2.1: Platelet response at sites of vascular injury. When a vascular injury occurs, the subendothelial matrix beneath endothelial cells becomes exposed. Within this matrix are bound vWF and collagens. Platelets in the bulk flow tether to the matrix bound vWF via their GPIbα receptors. These tethers are either converted to rolling on the vWF at the site of injury or the platelet flows freely downstream to either return to the bulk flow or tether to another bound vWF molecule. Platelet rolling is converted into firm adhesions upon platelet activation, when the $\alpha_{IIb}\beta_3$ integrin is exposed and binds firmly to the matrix molecules. Additional platelets and soluble vWF molecules are then recruited to the site of injury where vWF acts to bridge platelets and collagen and a hemostatic plug is formed.

Tethering is the process by which platelet velocity is reduced and is mediated by rapid kinetics of binding between the two molecules. In order for platelets to roll on the vessel wall after being slowed, the binding between GPIbα and vWF must be mediated by fast on- and off-rates. These rapid kinetics for interactions between platelet GPIbα and vWF allow platelets to slow down and stay at the vessel wall for the time needed for tethering events to be converted into firm adhesions. Figure 2.1 shows this process.

In tethering events, GPIbα-vWF interactions allow platelets to transiently bind to the vessel wall during injury. The platelets can then either break loose or the tethering can be converted into rolling. Transient tethering results in a reduction in platelet velocity compared to free-flowing platelet velocity. The reduced velocity of platelets in turn allows them to continuously interact with the vessel wall. It has been suggested that the activated platelet undergoes a conformational change revealing the $\alpha_{IIb}\beta_3$ integrin. The activated $\alpha_{IIb}\beta_3$ integrin then interacts with vWF, fibrinogen, and other subendothelial matrix proteins such as vitronectin and fibronectin at the vessel wall resulting in stable adhesion of platelets [9]. Following firm adhesion of platelets, they are activated through a series of signaling events, which leads to platelet spreading across the exposed surface, granule release, platelet aggregation, and recruitment of additional platelets and soluble vWF from the plasma to form a hemostatic plug [10].

2.2 von Willebrand Disease

In von Willebrand diseases, which result in patient bleeding, mutations in the vWF molecule change the vWF molecule's ability to bind platelet GPIbα properly. Several

types of VWD have been observed and are separated into three major types: 1, 2, and 3. In type 1 VWD, patients have low levels of vWF antigen, but the vWF present binds normally. In type 2 VWD patients have defective vWF binding, where there is either enhanced or reduced binding between vWF and its binding partner. Type 2 VWD is further separated into type 2A (decreased number of large vWF multimers), type 2B (increased binding to platelet GPIbα), type 2M (decreased binding to platelet GPIbα), and type 2N (decreased ability to carry Factor VIII). In type 3 VWD, patients lack vWF protein [11]. For this thesis research, we are interested in how vWF and GPIbα interact together, so we have chosen to study mutations causing type 2B and type 2M VWDs.

2.2.1 Type 2B VWD

Type 2B VWD results from a qualitative defect in the vWF-A1 domain. These mutations result in an increase in the binding between vWF and platelet GPIbα in the presence of ristocetin and are defined as gain-of-function mutations [12, 13]. It is believed that this increased binding is not due to normal triggers such as vascular injury and increased shear stress. A loss of hemostatically active high molecular weight multimers has been observed in type 2B VWD [11]. Further, this increased binding between platelets and vWF results in the clearance of platelets and, hence, mild thrombocytopenia. Figure 2.2 shows the platelet response at sites of vascular injury when type 2B VWD mutations are present. Here platelets and mutant vWF form aggregates in the bulk. This model is in agreement with the observation that circulating platelets are coated with vWF molecules that have the type 2B mutation [11]. With platelets sequestered in these aggregates, there are few available to act at sites of vascular injury, which leads to patient bleeding.

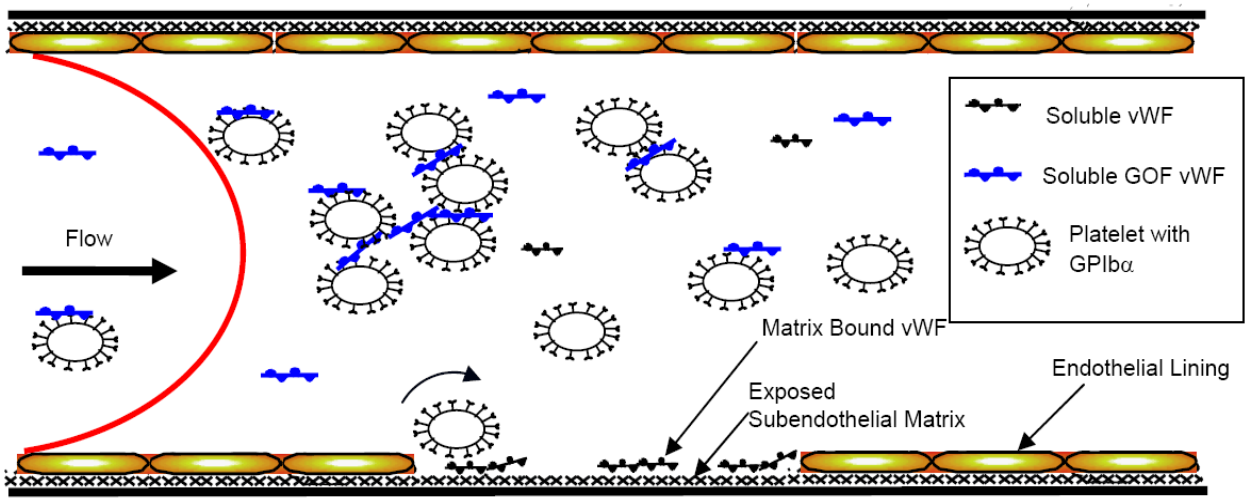

Figure 2.2: Platelet response at sites of vascular injury while type 2B VWD mutations are present in the vWF molecule. As with the normal case in Figure 2.1, when a vascular injury occurs, the subendothelial matrix beneath endothelial cells becomes exposed. Platelets in the bulk flow interact with soluble vWF rather than tethering to the matrix bound vWF via their GPIbα receptors. Because platelets are sequestered in these platelet/vWF aggregates, they are unable to tether at sites of injury. The result is that there are fewer platelets available to initiate rolling interactions at the injury site, resulting is delayed hemostatic plug formation, which results in bleeding.

2.2.2 Type 2M VWD

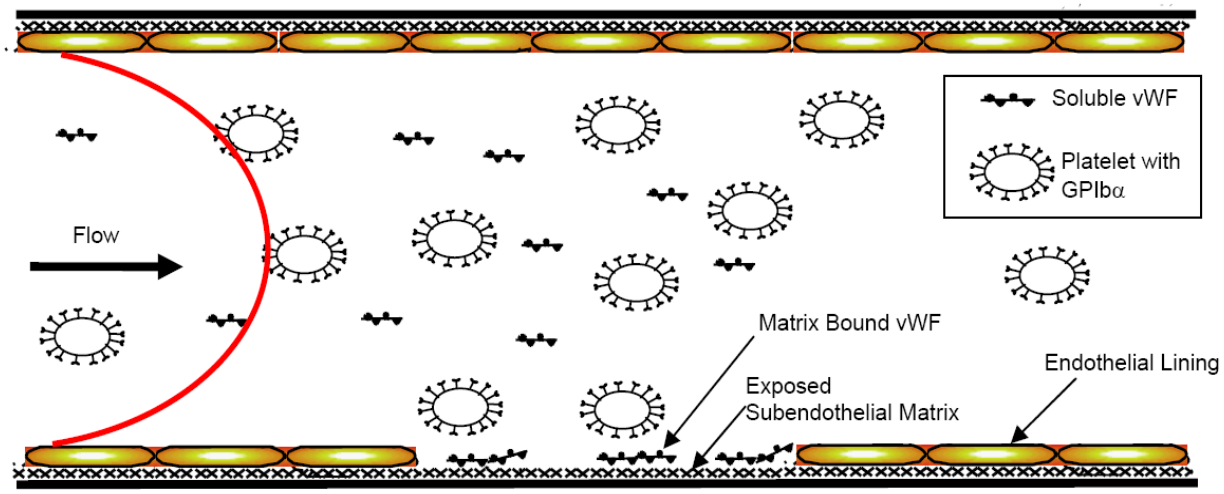

Figure 2.3: Platelet response at sites of vascular injury while type 2M VWD mutations are present in the vWF molecule. As with the normal case in Figure 2.1, when a vascular injury occurs, the subendothelial matrix beneath endothelial cells becomes exposed. Platelets in the bulk flow do not interact with soluble vWF. However, they also are less likely to tether to the matrix bound vWF via their GPIbα receptors. Because platelets are less likely to bind matrix bound vWF, they are unable to tether at sites of injury. The result is that there are fewer platelets available to initiate rolling interactions at the injury site, resulting in delayed hemostatic plug formation, which leads to bleeding.

Mutations causing type 2M VWD result in enhanced bond dissociation and increased rolling velocities. Further, these mutations are defined as LOF because they display reduced ristocetin induced binding. The G561S type 2M mutant displays decreased ristocetin binding and normal multimer number, formation, and pattern [6]. Further, this mutation may prevent a conformational change in the vWF molecule that reveals the GPIbα binding site [7]. Here, in Figure 2.3, we model the binding behavior for platelet interactions with vWF carrying LOF type 2M VWD mutations. Because of the decreased binding affinity, there are fewer platelets that will make bonds at the site of vascular injury. Because fewer platelets make successful interactions at the site of vascular injury, the site heals more slowly than normal and the patient bleeds.

2.3 Platelet-Type von Willebrand Disease

Mutations in platelet GPIbα have also been observed that result in bleeding similar to that seen in patients with type 2B VWD. When the mutation is in platelets, the diseased is called pt-VWD. Theses mutations result in increased binding between vWF and platelet GPIbα as is the case for type 2B VWD. The binding mechanism underlying patient bleeding is thought to be similar to that seen for type 2B VWD [14] and is modeled here in Figure 2.4.

2.4 Bernard Soulier Syndrome

Bernard Soulier Syndrome results from defects in the GPIbα molecule that result in decreased adhesion between platelets and vWF. This disease is characterized by increased bleeding time, lack of ristocetin induced platelet aggregation, a decreased

number of platelets, enlarged platelets, and thrombocytopenia. Further, it has been observed that some variants have normal levels of defective GPIbα present leading to decreased binding to vWF, while other variants have decreased levels of GPIbα expressed [15].

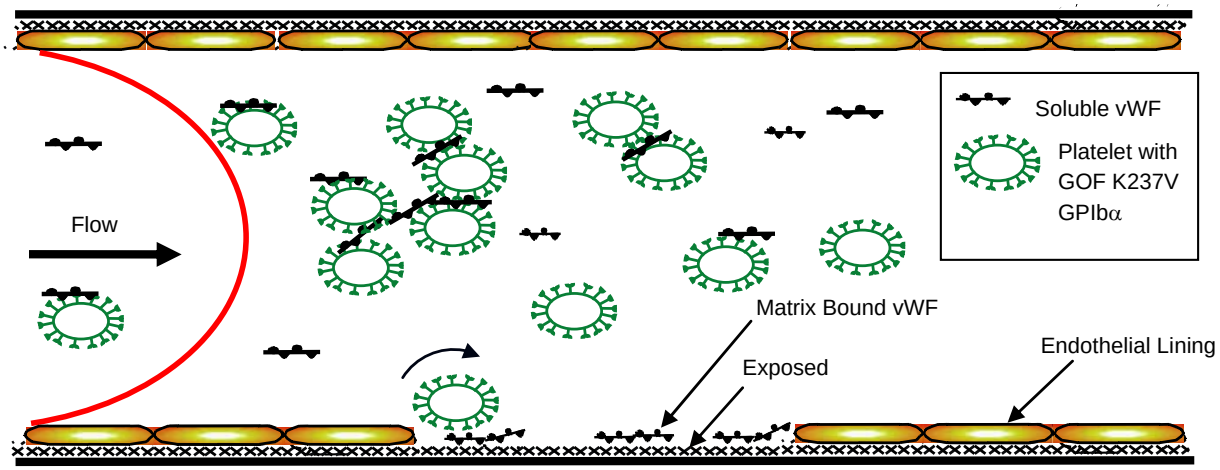

Figure 2.4: Platelet response at sites of vascular injury while platelet type VWD mutations are present in the GPIbα molecule. As with the normal case in Figure 2.1, when a vascular injury occurs, the subendothelial matrix beneath endothelial cells becomes exposed. Platelets in the bulk flow interact with soluble vWF rather than tethering to the matrix bound vWF via their GPIbα receptors. Because platelets are sequestered in these platelet/vWF aggregates, they are unable to tether at sites of injury. The result is that there are fewer platelets available to initiate rolling interactions at the injury site, resulting is delayed hemostatic plug formation, which results in bleeding.

2.5 Parallel Plate Flow Chamber Model System

Parallel plate flow chambers are a common *in vitro* method for studying the effects of steady, laminar fluid shear stress on the interactions between two adhesion molecules. In flow chamber experiments, cells expressing either the receptor or its ligand are typically perfused through a parallel plate flow chamber across the respective ligand or receptor coated surface. In these experiments data taken include rolling velocities, tether rate, and pause times. Additionally, flow chamber systems can be used to determine kinetic bonding parameters by measuring transient tethering lifetimes and tethering frequency.

The transient tether lifetime is used to measure the off-rate, while the tethering frequency is used to measure indicate changes in the on-rate [16]. Pause time analysis is used to determine the kinetic off-rate. In this technique the ligand is coated at a density such that only individual tethering events can occur – i.e., too low a ligand coating density for rolling to occur. To obtain the off-rate, the tether distribution data is fit to a first order kinetics equation [16].

$$dN_b = -k_{off}N_b \qquad \text{(Equation 1)}$$

N_b is the number of cells remaining tethered

k_{off} = off-rate, negative of the slope

In addition to pause time analysis to determine off-rates, tethering frequency is used to measure kinetic on-rate indicators, and, more specifically, the number of tethering event within a given time frame. These techniques have been used to observe the kinetics in many adhesion molecule systems: P-selectin glycoprotein ligand-1 (PSGL-1)-L-selectin [17], PSGL-1-P-selectin [18], neutrophils-P-selectin [19], neutrophils-E-selectin [19], neutrophils-L-selectin [19], and GPIbα-vWF [16, 20, 21].

The parallel plate flow chamber system has been used by several researchers to observe GPIbα-vWF interactions. Using a parallel plate flow chamber apparatus, Doggett and co-workers first showed that the GPIbα-vWF bond for platelets interacting with GOF I546V vWF-A1 had a decreased off-rate compared to wt vWF-A1 [21], which contradicted previous biochemical assay data by Miura and colleagues that showed an increase in on-rate was responsible for enhanced adhesion [22]. Later, Doggett et al. showed that interactions between GOF GPIbα and wt vWF were due to both an increased on-rate and a decreased off-rate [23]. This trend, where on-rate increases and off-rate

decreases, was also shown by Kumar and co-workers using CHO cells expressing GPIbα or CHO cells expressing GOF mutant GPIbα rolling on wt vWF-A1 [16].

2.6 vWF and GPIbα Molecules: Function and Structure

2.6.1 The vWF Molecule

Platelet adhesion and aggregation are mediated by vWF and GPIbα of the platelet GPIb-IX-V complex. VWF is the largest soluble protein found in the plasma and as a soluble plasma protein, vWF does not interact with platelets. VWF is also found in α-granules of platelets and subendothelial matrices [24]. At high shear stress vWF binds to exposed subendothelial matrix materials and functions to bridge exposed subendothelial collagens and circulating platelets. It has been suggested that exposure to high shear stress upon binding to collagen results in a conformational change in the vWF subunit, resulting in a form of vWF that is active and able to form functional interactions with platelets [25].

VWF is a multimeric glycoprotein consisting of a repeating vWF dimer with a molecular weight of 500 kDa [26]. The vWF molecule found in the plasma is a globular protein, and is a multimer of the vWF dimer [27] with a molecular weight ranging from 500 to 20,000 kDa [28]. Plasma vWF is predominately high molecular weight multimers [29]. A single vWF monomer contains 2,050 amino acids and consists of 11 domains: D'-D3-A1-A2-A3-D4-B1-B2-B3-C1-C2. The mature subunit is decorated with 12 N-linked and 10 O-linked carbohydrates [30]. The function of N-linked and O-linked oligosaccharides on vWF remains unclear. Some studies have indicated that these

carbohydrate chains are responsible for enhanced platelet aggregation [31], while other studies have shown these chains to have an inhibitory role in GPIbα aggregation [32].

Each of the domains within the vWF subunit has distinctive activities. Factor VIII, a protein involved in the clotting cascade, binds vWF at the N-terminal D domains [33]. The A1 domain has been shown to be the binding site for GPIbα in the GPIb-IX-V complex [24], non-fibrillar collagen type IV [34], collagen type I [7, 35], collagen type III [7, 35], heparin [36], ristocetin, botrocetin, and bitiscetin [37]. The A3 domain is the binding site for fibrillar collagens types I [38] and III [39]. Ristocetin is an antibiotic which is often used in vitro to study platelet agglutination [40]. Botrocetin and bitiscetin are two snake venoms which induce platelet agglutination via interactions with vWF. Crystal structures for both the A1 and A3 domains have been elucidated to obtain a better understanding of these binding sites [39, 41, 42]. Finally, the vWF-C1 domain contains an RGD binding site, to which platelet integrin $\alpha_{IIb}\beta_3$ has been shown to bind [43].

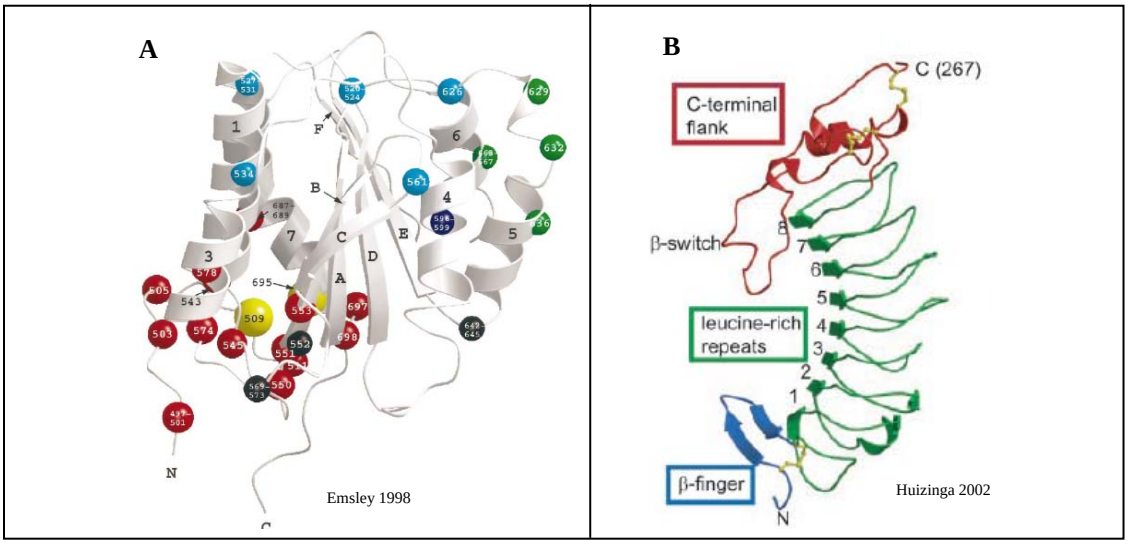

Figure 2.5: Platelet GPIbα and vWF-A1 crystal structures: isolated vWF-A1 domain [39] (A) and the N-terminus of GPIbα [27] (B).

As can be seen in Figure 2.5*A* [39], the A1 domain of vWF consists of a central hydrophobic parallel β-sheet flanked by amphipathic helices, containing 7 helices and 6 strands [39]. A disulfide bond constrains this domain into a globular structure by linking the C-terminal and N-terminal regions [27, 39] at Cys^{509}-Cys^{695} [39]. Short extensions which protrude away from the globular structure are formed on the surface containing the N- and C-termini. It is on this surface that all type IIb VWD mutations are clustered [39]. In soluble vWF, multimers are in a coiled conformation that shields the A1 domain [25]. However, when the A1 domain is bound to GPIbα the N-terminal extension is shifted in a way which reveals more of the surface of the globular domain [27]. It has been suggested that the β1-α2 loop in the vWF-A1 molecule is largely responsible for changes in interactions between GPIbα and vWF [8].

2.6.2 The GPIbα Molecule

The receptor for the vWF ligand is found in the GPIb-IX-V complex on platelets. This complex consists of four transmembrane polypeptides, GPIbα, GPIbβ, GPIX, and GPV. The complex contains two of each of GPIbα, GPIbβ, and GPIX arranged symmetrically around one GPV, with a disulfide bond between the α and β subunits (reviewed by López [44]). It has been shown that vWF binds to the GPIbα subunit in the GPIb-IX-V complex [45]. GP1bα is a highly glycosylated transmembrane protein, which has been implicated in binding to vWF [46, 47], MAC-1 [48], α-thrombin [49], and P-selectin [50].

GP1bα protrudes from the platelet surface via a highly glycosylated stalk extending approximately 45 nm from the cell surface [51]. This stalk, from residues 303

to 485, has O-linked carbohydrates attached to almost every third or fourth residue and is followed by a hydrophobic transmembrane domain from residues 486 to 514 and a cytoplasmic tail from residues 515 to 610. This cytoplasmic tail contains binding sites for both intracellular signaling molecules and actin binding proteins [52, 53]. GP1bα mutants with truncated cytoplasmic tails rolled faster than wild type [54], indicating the cytoplasmic tail is important not only for signaling but also in modulating cell rolling behavior. This implicates GP1bα as not only a cell adhesion molecule, but also as a molecule involved in signaling and cell structure.

The crystal structure of the N-terminus of the complete GP1bα molecule has been determined (residues 1-279) (Figure 2.5*B*) [55]. This region of GP1bα consists of an N-terminal β-hairpin (residues 2 – 18), 8 leucine rich repeats (LRRs), (residues 19 – 204), a disulfide bonded loop region (residues 205 -264), and a C-terminal anionic region (residues 265 – 280) [55]. The N-terminus of GP1bα is composed of two disulfide loop structures [15] flanking 8 LRRs [27]. Within the disulfide loop region residues 227 – 241 form a β-switch [27], which protrudes outward from the concave face formed by residues 1 – 279 [55]. At the base of this N-terminal region lie three sulfated residues [56], which are required for binding to both vWF and α-thrombin [57-59]. Tait et al. showed that the residues surrounding these tyrosines are important factors for sulfation [60]. This region is followed by a series of negatively charged residues from residue 282 to 302.

Crystal structures suggest that the β-switch (cystine loop) and β-finger (N-terminus) strands of GPIbα bind directly to vWF-A1. Upon binding to vWF-A1, the region between residues 227 and 241 at the C-terminus of the GPIbα fragment undergoes a conformational change [27]. Many pt-VWD mutations are found in the β-switch region

of the GPIbα molecule, while LOF, Bernard-Soulier mutations are found in the LRR region [27, 55]. VWF-A1 mutations located on the A1 molecule's surface containing its N- and C-termini align with the N-terminal β-finger residues in the GPIbα molecule [27].

2.7 Role of ADAMTS-13

ADAMTS-13 is a protease present in the plasma that cleaves ultra large forms of the vWF molecule at its A2 domain between residues Y1605 and M1606 [61]. Ultra large forms of vWF are secreted by endothelial cell Weibel Palade bodies onto the endothelial surface where they undergo a conformational change and become elongated due to conditions of high shear stress. In their elongated forms the A2 domain is exposed, allowing the ADAMTS-13 enzyme to cleave the ultra large form of vWF into smaller forms, which are then released from the surface and become soluble vWF [25, 62, 63]. Further, when soluble vWF binds at sites of vascular injury, it is subjected to high shear stresses causing it to unfold revealing both the A1 and A2 domains. It is thought that the ADAMTS-13 protease plays a role in regulating thrombus formation during the injury repair by cleaving vWF at its exposed A2 domain preventing the thrombus from becoming too large [64]. Defects in ADAMTS-13 result in patients who have ultra large forms of vWF circulating in the plasma. The presence of these large vWF forms results in thrombus formation and is seen in thrombotic thrombocytopenic purpura (TTP) [65].

2.8 Biomechanics of Interactions Between Adhesion Molecules Under Flow

Blood cell adhesion molecules interact while subjected to fluid flow applied forces. These types of interactions have been studied using parallel plate flow chambers and

several important observations for these adhesive interactions under flow have been made. Of particular relevance to the work presented in this dissertation are the shear threshold phenomena, the observation of catch bonds, and the need for high-speed video microscopy. Each topic is discussed in greater detail in this section.

2.8.1 Shear Threshold

While measuring rolling velocities, several researchers have observed that at very low shear rate values there appears to be no rolling. However, as the shear rate is increased, rolling begins. This concept has been termed the shear threshold phenomena because a threshold level of shear rate is required in these systems to promote rolling, and hence, any subsequent adhesive events. This shear threshold concept has been shown for several systems, beginning with those involving L-selectin interacting with both neutrophils and T-lymphocytes. Neutrophils and T-lymphocytes were rolled across peripheral node addressin (PNAd - a surface containing L-selectin) and it was shown that as shear rate was decreased there was a decrease in rolling velocity to no rolling at a non-zero shear rate value, indicating that the cells required a threshold level of shear rate in order to roll. However, unlike the L-selectin surface, a shear threshold for P- and E-selectin were not seen in this research [66], but later work by Lawrence et al. showed a threshold for all three selectins: P-, E-, and L-selectin [67]. It has been shown that selectins bearing single mutations in either the hinge region between L-selectin's lectin and EGF domains have a reduced shear threshold [68], while mutations in the ligand binding surface of the L-selectin molecule result in elimination of the shear threshold requirement [69]. It has been shown that GPIbα expressed on the platelet surface rolls on

vWF exposed during vascular damage only above a threshold value of shear rate [21], which corresponds to arterial flow rates [21, 70]. Further it was shown that this shear threshold was lost for platelet interactions with GOF I546V vWF-A1 mutant [21]. More recently the shear threshold phenomena has also been observed in bacteria. Here it was seen that the FimH molecule found on *E. coli* bacteria rolls on mannose only above a shear threshold [71, 72]. Recently the shear threshold concept has been linked to that of a transition point in systems where a catch bond exists for interactions with selectins and their ligands. In these systems, this optimum threshold occurs when increasing shear force results in a switch from increasing bond lifetimes to decreasing bond lifetimes [17].

There are two prevailing hypotheses that have been developed to explain these physiological observations that there is a shear threshold. One hypothesis thought to explain the shear threshold phenomenon is that bond formation is enhanced by a flow-dependent increase in the on-rate [73, 74], while the second hypothesis is that catch bonds exist, which slow the dissociation rate [17, 18, 75]. In the first hypothesis, there are two theories. One is that bond formation is enhanced by a flow-dependent increase in the on-rate due to a shear rate dependent transport of adhesion molecules to their ligands so that new bonds can form before old ones are able to dissociate [73, 74]. The other theory is that bond formation is enhanced by a flow-dependent increase in the on-rate due to shear stress dependent increase in the cell surface contact area, which would allow more adhesion molecules to come into contact with each other [67, 76, 77]. In the second hypothesis, a catch bond forms, the off-rate decreases, resulting in an increase in the bond lifetimes, which further results in stable rolling [17, 18]. Yago et al. are the first to

suggest that catch bonds are the mechanism for the shear threshold phenomenon based on experimental observations [17].

2.8.2 Catch Bonds

Since the theoretical prediction of catch bonds by Dembo et al. [75], many researchers have sought examples of catch bonds in biological systems. The first system in which catch bonds were observed was that of P-selectin and PSGL-1 [18]. Atomic force microscopy (AFM) and flow chamber experiments were used to explore P-selectin-PSGL-1 binding through bond lifetimes. Marshall and colleagues observed that the bond lifetime is first decreased by increasing force, but subsequently bond lifetime is increased with increasing force. This work not only is the first to show catch bond behavior with biological molecules, but it also shows that there exists a catch-slip transition force suggesting a mechanism for regulation of cell adhesion. Additionally, their data suggests that the transition from catch bonds to slips bonds governs rolling velocity across the shear threshold. They conclude that the role of the catch bond is to convert weak tethers to strong ones, enabling longer bond lifetimes.

In addition to P-selectin, another selectin family member, L-selectin, has been shown to adhere using catch bonds [78]. Again, for these experiments, AFM and flow chamber experiments were used. This work suggests that the catch bond mechanism contributes to the shear threshold phenomenon because catch bonds were observed below the threshold, while slip bonds were observed above the threshold. Here catch bonds are defined as a decrease in the off rate and slip bonds are defined as an increase in the off rate, as also described by Dembo et al. [75].

Another system in which catch bonds are thought to exist is that of FimH on *E. coli* binding to guinea pig red blood cells as a test of adhesion [71, 79]. The FimH molecule is located on the tips of the appendages of the bacteria's pili and binds to manomannose residues. It was observed that FimH found on uropathogenic *E. coli* was able to bind manomannose residues under static conditions, whereas, this binding is seen rarely in intestinal *E. coli*. Instead, intestinal *E. coli* adhesion via FimH has been seen to be enhanced by mucosal flow (shear flow), such as that seen in the selectin family [71]. Additionally, Thomas et al. have observed a decrease in the off-rate of the adhesion of FimH when external shear stress was applied [71], which is suggestive of catch bond behavior [79].

Additionally, one research group has observed a catch bond like conformational change in a system in which standard biomechanical methods have not been used to elucidate the presence of catch bonds [80]. Here, FRET (fluorescence resonance energy transfer) is used to observe the structural transformation in the integrin α_4 in response to stimulation using divalent cations and cells. It was seen that there was a vertical extension in the integrin, suggesting a conformational change. Concurrently there was seen a change in binding affinity. These results taken together suggest a mechanism to explain the catch bond phenomenon.

2.8.3 High-speed Video Microscopy

It is thought that the use of high-speed video microscopy will give a more accurate description of the binding kinetics seen in adhesion molecule pairs. Indeed, Smith et al. suggest that the rolling steps are so close together that distinctions cannot be

seen between them, resulting in a false sense of the true measure of the kinetics [19]. The rationale for a higher speed is that it increases the temporal resolution, hence increasing the chance of observing binding events occurring faster than 30 frames per second (fps), which is the standard frame rate used by researchers. In these experiments higher temporal resolution was used to determine the kinetic off-rate as determined by parallel-plate flow chamber analyses. Binding kinetics of P-selectin, E-selectin, and L-selectin rolling on neutrophils were measured. A comparison between high-speed video microscopy results (obtained at up to 240 fps) with those measured using the traditional 30 fps showed that higher temporal resolution made a difference in the interactions observed for L-selectin binding. In contrast, the values obtained were similar for both 240 fps and 30 fps for P-selectin and E-selectin, suggesting that a greater frame rate may be important during observations of some interactions, though not all. Several other researchers have also used high-speed video microscopy in order to observe the kinetics between adhesion molecules. Yago and co-workers used this technique to observe the kinetics of L-selectin binding to PSGL-1 [17]. They use this higher temporal resolution technique to show that the catch bond is responsible for the shear threshold phenomenon.

CHAPTER 3: METHODS

3.1 Proteins and Antibodies

Recombinant vWF A1 molecules (wt, R687E, and G561S) and wt vWF-A1A2A3 molecules were produced as previously described [7, 81, 82]. Whole vWF was purchased from Calbiochem (San Diego, CA). FITC labeled human anti-GPIbα clone AK2 was purchased from Abcam (Cambridge, MA). FITC labeled calibration beads were purchased from Bangs Laboratories, Inc. (Fishers, IN).

3.2 CHO Cells Expressing GPIbα

Chinese Hamster Ovary (CHO) cells expressing wt GPIbα were produced as previously described [83]. These cell lines allow for the observation of the isolated GPIbα receptor and can be used to confirm GPIbα's role in the platelet interactions studied, because platelets have several molecules, including integrins, that may interact with vWF. Further, CHO cells were used for expression of GPIbα because they are robust cells that are easily transfected and cultured. Further, these cells are essentially spherical and allow for direct correlations with mathematical models and equations that assume spherical particles. CHO cells were cultured in α-MEM (Mediatech, Inc., Manassas, VA) containing 10% FBS (Hyclone, Logan, UT) and penicillin (5,000 units/mL)/streptomyocin (5,000 μg/mL) (Cellgro, Manassas, VA). Medium for all CHO

cell lines was supplemented with selection agents G418 (400 μg/mL, Invitrogen, Carlsbad, CA) and methotrexate (80 μM, Sigma, St. Louis, MO). Media for CHO cells expressing the GPIbα receptor (wt or mutant) was also supplemented with 400 μg/mL Hygromyocin B (Invitrogen, Carlsbad, CA). All cell lines were maintained at 37^{o}C in 5% CO_2, 95% air.

3.3 Platelet Isolation

Platelets were isolated from whole blood drawn from healthy volunteers according to an approved Institutional Review Board procedure, in which all volunteers gave written, informed consent. Platelet rich plasma was isolated from fresh whole blood and drawn into citrate buffer (25 g sodium citrate, 8 g citric acid, 500 ml H_2O) containing 2 μM prostaglandin E-1. Whole blood was centrifuged at 150g for 15 minutes at room temperature. The supernatant, platelet rich plasma, was removed and mixed with acid citrate dextrose (6.25 g sodium citrate·2 H_2O, 3.1 g citric acid anhydrous, 3.4 g D-glucose in 250 ml H_2O), 10% by volume, and centrifuged at 900g for 5 minutes at room temperature. The pellet was suspended in Hepes-Tyrode buffer and diluted to $1x10^8$ platelets per mL in Hepes-Tyrode buffer for flow assays.

3.4 Measurement of Viscosity

Viscosity of platelet suspension buffer was measured using an Ostwald dripping viscometer as previously described [17] and at 37^{o}C. Buffer alone and buffer plus 6% Ficoll were added to the reservoir of an Ostwald dripping viscometer. The time taken for the fluid to fall from the top of the capillary bulb to the bottom was measured. Density

for Ficoll was provided by the manufacturer at 1.02 g/mL for 6% Ficoll. The viscosity of the buffer plus 6% Ficoll was calculated relative to buffer alone using Equation 2.

$$\mu_{6\%} = \left(\frac{\Delta t_{6\%}}{\Delta t_{0\%}}\right)\left(\frac{\rho_{6\%}}{\rho_{0\%}}\right)\mu_{0\%} \qquad \text{(Equation 2)}$$

μ = viscosity of fluid

Δt = time for fluid drop in viscometer capillary bulb

ρ = density of fluid

In some experiments 6% Ficoll (MW 400, Sigma) (w/v) was added to increase the viscosity 1.8 times compared to buffer alone.

3.5 Preparation of vWF Molecule Coated Surfaces

The flow chamber surface was a 35 mm tissue culture dish coated with vWF A1 molecules (wt at 100 μg/mL, R687E at 100 μg/mL, or G561S at 200 μg/mL), wt vWF A1A2A3 (at 100 μg/mL), or whole vWF molecules (at 50 μg/mL). A 20 μL drop of vWF molecule was coated onto the dish and incubated overnight at 4^{o}C. The surface was rinsed with PBS and blocked with 20 μL of 1% HSA for 2 hours at room temperature, then the surface was again rinsed with PBS. The prepared dish was used as the lower surface for the flow chamber and brought to 37^{o}C prior to starting the experiment.

3.6 vWF-A1 Site Density Measurements

The site density (number of vWF-A1 sites per μm^2) of vWF-A1 molecules was determined using an ELISA previously described [16]. VWF-A1 molecules were coated onto the surface of a 96-well tissue culture plate. Horseradish peroxidase (HRP)-

conjugated 6-his-tag antibody was used to detect the 6-his-tag attached to the recombinant vWF-A1 molecules. HRP absorbance was measured at 490 nm and was that of o-phenylenediamine/H_2O_2. A calibration standard was used to quantify the number of sites per unit area.

3.7 Flow Cytometry for GPIbα-Receptor Expression on CHO Cells and Platelets

Surface expression of the GPIbα receptor on platelets was determined using a primary conjugated antibody to GPIbα. The antibody is specific for the N-terminus of the GPIbα molecule, clone AN51 or clone AK2 [28]. Calibration beads (Bangs Labs, Inc.) were used to zero the flow cytometer voltage settings, such that the blank bead population is at the origin of the mean fluorescence intensity vs. count graph. The mean fluorescent intensity of each bead population was then measured and the number of receptors per surface area was calculated using the calibration beads.

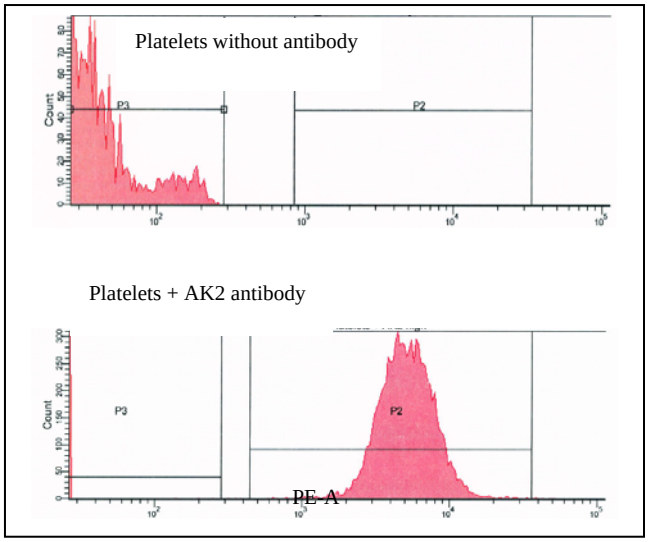

Figure 3.1: GPIbα expression on platelets as assessed by flow cytometry. Platelets were labeled with and without primary RPE-conjugated GPIbα antibody (clone AK2). Platelets without antibody showed background low fluorescent values, while platelets with antibody showed a significantly increased fluorescent value. These results indicate that the GPIbα molecule is present on platelets.

Figure 3.1 shows representative histograms for platelets with and without antibody and indicates that we are able to detect the GPIbα receptors on platelet samples. Platelets without antibody were used as a control. Platelets were counted and sized using a Coulter Counter. The average diameter from this method was used to determine the surface area of the platelet sample, which was used to calculate the number of receptors per surface area of cell.

Surface expression of the GPIbα receptor expressed on CHO cells was also determined using the same primary conjugated antibody to GPIbα as was used for platelet GPIbα expression levels.

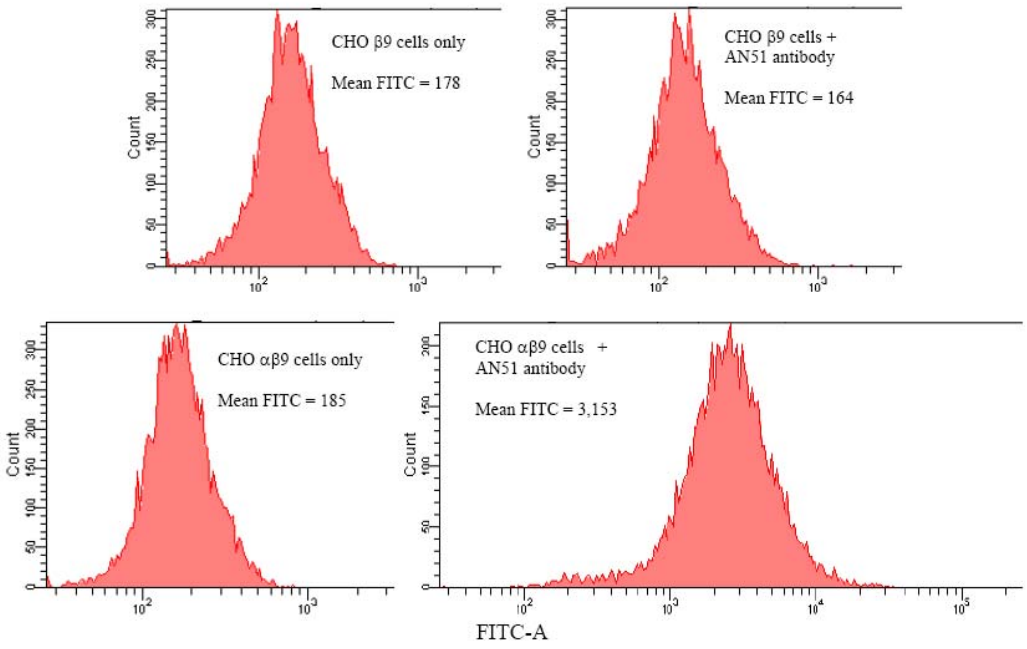

Figure 3.2: Flow cytometry for GPIbα expression on CHO αβ9 cells. CHO β9 or CHO αβ9 cells were labeled with or without primary conjugated FITC-AN51 GPIbα antibody. CHO β9 cells without antibody, CHO β9 cells with antibody, and CHO αβ9 cells without antibody showed background low fluorescent values, while CHO αβ9 cells with antibody showed a significantly increased fluorescent value. These results indicate that the GPIbα molecule is present on CHO αβ9 cells and not on control cells, CHO β9.

CHO cells were suspended in PBS at a concentration of 0.5 x 10^6 cells/mL. CHO αβ9 cells were incubated for 30 minutes with a primary conjugated GPIbα antibody. Three control populations were used, all of which resulted in mean fluorescent values near zero: CHO β9 cells without antibody, CHO β9 cells with antibody, and CHO αβ9 cells without antibody. Figure 3.2 shows an example set of flow cytometry histograms where GPIbα receptors were labeled with a FITC labeled primary conjugated antibody directed to the AN51 clone site on GPIbα. Here it is clear that CHO αβ9 have the GPIbα receptor present, while CHO β9 and unlabeled controls show only background fluorescence.

3.8 Flow Cytometry Cell Sorting to Maintain Receptor Cell Surface Expression

Flow cytometry was used as described above to maintain the surface expression of GPIbα on CHO cells in order to ensure that multiple experiments using CHO cells may be combined and/or compared. Calibration beads from Bangs Labs, Inc. were used to determine the number of receptors per surface area for CHO αβ9 cells, which were sorted using either the FITC-AN51 antibody or the RPE-AK2 antibody, to maintain an expression level similar to that seen on the platelet surface measured as number of receptors per μm^2 [16].

3.9 Flow Chamber Assay

A parallel platelet flow chamber (GlycoTech, Gaithersberg, MD) was used to apply shear stress to platelets interacting with a vWF coated surface. Cells (CHO β9 or CHO αβ9) or platelets were perfused through the flow chamber with a syringe pump (Harvard Apparatus, Holliston, MA). Figure 3.3 shows this flow chamber set up. Interactions

were visualized using an inverted-stage phase-contrast microscope (DIAPHOT-TMD; X-20 or X-10 phase objective and X-5 projection lens, Nikon, Garden City, NY). The flow chamber was maintained at 37^{o}C using an air curtain surrounding the microscope. Images were captured at 250 fps directly to a computer using a high-speed video camera and Phantom 640 software (Phantom V4.2, Vision Research, Inc., Wayne, New Jersey).

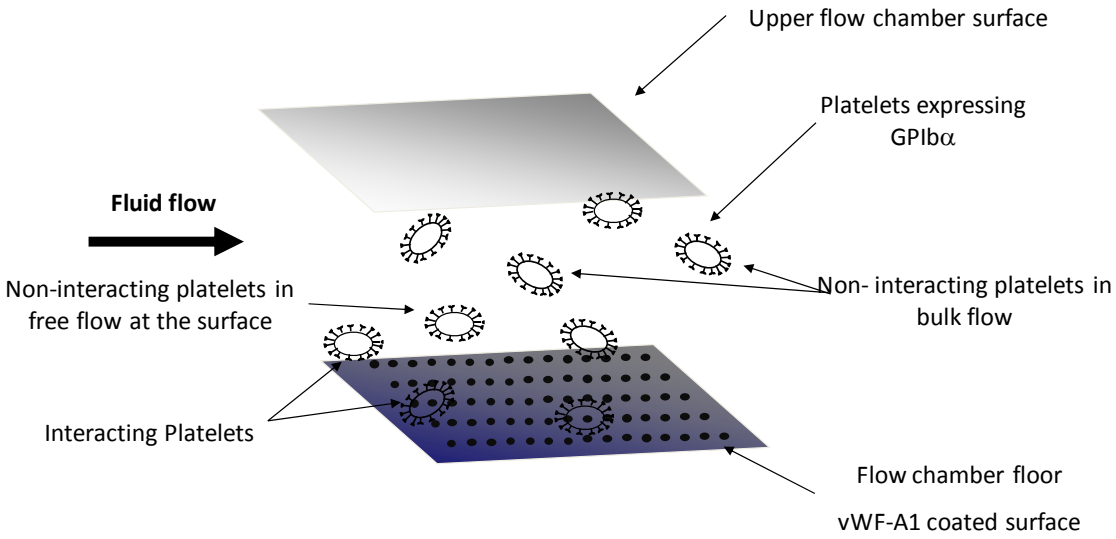

Figure 3.3: Parallel plate flow chamber system. Platelets or CHO cells expressing GPIbα are perfused across a vWF coated surface. Cells recorded are observed in multiple fluid layers and are classified as cells interacting at the lower (vWF molecule coated) surface and cells that are not interacting in the bulk flow.

Images were analyzed post-experiment using the Track Object module in Metamorph Offline software (Molecular Devices, Sunnyvale, CA). Further data analysis, plot generation, and statistics were completed using a Matlab analysis program written specifically for analysis of this data. For this analysis, the position for each frame was determined during data collection when cells were tracked. This position was used directly to determine velocity for each frame as distance per time. Lower bounds for

rolling velocities were determined by tracking cells that were stopped in each video. The velocity associated with these cells was then subtracted from cells that were rolling to determine the velocities for rolling cells. For rolling parameter analysis, position and time data for each frame were used as inputs into the stop-go model described previously [17] and discussed here in Methods Section 3.13.

3.10 Flow Chamber Experimental Controls

The control coverslip was coated with 1% HSA. In experiments where CHO cells are used, CHO β9 cells, which do not express the GPIbα receptor, will serve as control for CHO αβ9 cells. Table 3.1 shows the components of CHO cell lines used.

Table 3.1: Cell lines used for flow chamber experiments.

Cell Line	Components
CHO β9	GPIb β and IX
CHO αβ9	GPIb α, β, and IX

3.11 High-speed Video Microscopy

Interactions of CHO cells or platelets interacting with vWF-A1 coated coverslips were recorded at 250 fps using a high-speed video camera. To determine if 250 fps was the optimal frame rate for the GPIbα-vWF interaction, frame rates ranging 100 to 500 fps were tested. The optimal frame rate (here 250 fps) was chosen such that rolling velocity and other parameter values no longer change as a result of further increasing the frame rate.

3.12 Treatment with ADAMTS-13 Enzyme

For experiments conducted in the presence of ADAMTS-13, the procedure is similar to that for other flow chamber experiments as described in section 3.9. For these studies whole vWF was coated on the 35 mm tissue culture dish overnight at 4^{o}C. The next day the dish was rinsed with PBS and coated with 1% HSA for 3 hours at 4^{o}C. The dish was again rinsed with PBS and the ADAMTS-13 enzyme (5 μg/mL) was coated on the whole vWF coated surface for 30 minutes at room temperature. The dish was then used as the bottom of the flow chamber assembly and platelets were perfused through the flow chamber and the transient tethering interactions recorded for analysis.

3.13 Measurement of Rolling Velocities and Rolling Step Parameters

Rolling velocities were calculated as the total distance traveled in a one second interval. Each velocity represents an average of tens to hundreds of cells. Rolling step parameters were determined as described [17] from video taken at 250 fps. In these studies rolling interactions were studied to gain insight into bonding behavior.

It has been established that cell rolling is predominately mediated by the dissociation rate of the bonds formed and broken during rolling motions [17, 21, 84]. Bond dissociation occurs because of the fluid force applied to the bond and is used to determine bond lifetime, which is inversely proportional to the dissociation rate. Because of these observations, when we observe a decrease in rolling velocity, it is reasonable that such an observation would suggest that the bond lifetime is increasing or that the dissociation rate is decreasing, which is indicative of a catch bond. These changes in bonding would result in a longer lived bond, which likely explains why the cell rolls more slowly.

Conversely, when the cell rolling velocity increases with increasing shear stress, it likely indicates that the bond lifetime is decreasing, or that the dissociation rate is increasing, which is indicative of a slip bond. For the purposes of the data presented in this dissertation, the term catch-slip is used to describe indirect bonding measurements of rolling interactions where it is likely that catch and slip bonds are present, rather than to indicate that catch and slip bonds were directly measured.

To further investigate rolling interactions, a more detailed analysis was conducted using the stop-go model for measurement of rolling step parameters, which is shown in Figure 3.4.

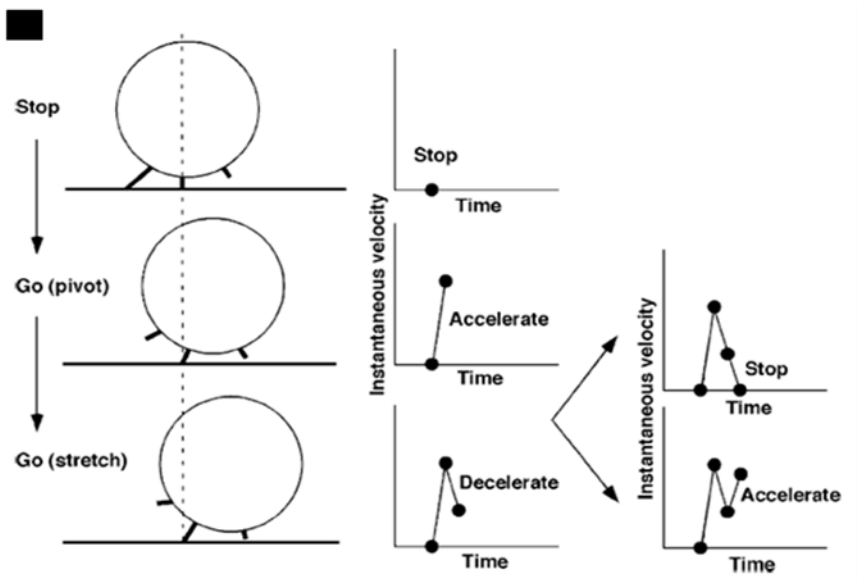

Figure 3.4: Rolling step parameter model from Yago et al. [17]. As a cell rolls on a surface, the shear force and torque generated by the fluid flow are counteracted by tensile and compressive forces. If these forces equally balance, the cell will stop. Otherwise, the cell can accelerate or decelerate depending on which set of forces dominates the rolling interaction for a given step. A frame-by-frame analysis was conducted and each frame was labeled as stopped, pivoting, or stretching.

Stop-Go analysis using this model has previously been used to describe the behavior of cells rolling on a ligand coated surface [17]. In this model, shear stress applied in a flow chamber results in shear force and shear torque applied to flowing and interacting cells.

When a cell tethers these parameters are balanced by a tensile force (trailing edge of the cell) and by a compressive force (due to contact area at the cell-surface interface). In order for cells to stop, the bond formed between the flowing cell and the stationary surface must be able to withstand the maximum values of shear force and shear torque. If this balance occurs the cell will stop. When this bond breaks the cell will accelerate, and as it does so, it will pivot in the direction of forward motion. Next, the cell will either stop again (if the balance of force and torques is met) or it will continue to accelerate. If a new upstream bond is formed the cell will decelerate. At each stage the cell may accelerate, decelerate, or stop depending on the amount of force a given bond provides to balance the shear force and shear torque. Based on these observations, a cell's motion for a given frame is characterized as a stop, pivot, or stretch and the time for each parameter is calculated.

3.14 Calculation of Transient Tethering Lifetimes

The bond lifetimes were calculated from transient tethering flow chamber data. Cells were observed and the time from when the cell stopped until the time where it returned to free flow was measured. These times were then used to generate a plot of the ln (# bound) versus the time the cell spent stopped. Figure 3.5 shows a representative plot. This type of plot was made for a single shear stress. The slope of the line is the kinetic dissociation rate, or off-rate, for the interactions. Further, the bond lifetime is inversely proportional to the off-rate, so can be calculated as $1/k_{off}$.

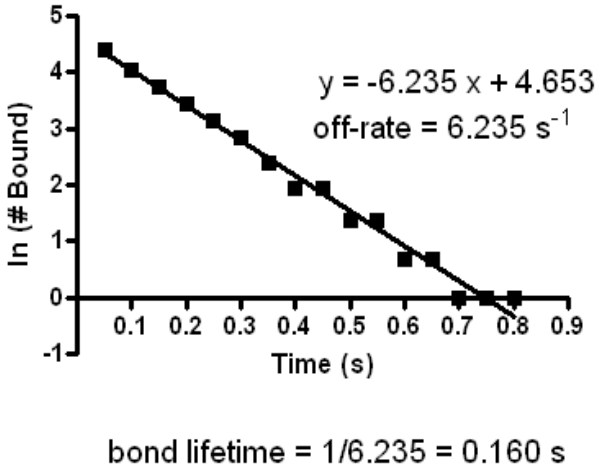

Figure 3.5: Determination of bond off-rates and calculation of bond lifetimes. Here an example set of cells at a single shear stress are shown to represent the calculation of off-rate. The number of cells bound was plotted versus the duration of the bond. The kinetic off-rate is slope of the line and the bond lifetime is the inverse of the off-rate.

3.15 Calculation of Shear Stress and Bond Force

The force on a bond under fluid shear stress can be converted into shear stress using the Goldman equations [1] and force and torque balances [16, 21, 84, 85]. First, the shear force formula from the Goldman equations is used to calculate shear force [1]:

$$F_S = 6\pi\mu Rh\gamma A \qquad \text{(Equation 3)}$$

Parameters and constants in these equations are as follows:

μ = viscosity (poise)

R = cell diameter (μm)

h = distance from the center of the cell to the wall (μm)

γ = shear rate (s^{-1})

A = Constant determined from Table I (a = R, h = h) in [1]

For this calculation, it is assumed that h/a approaches 1, so that A = 1.7005. Next, the resulting value from equation 3 is used in the following force and torque balances, respectively:

$$F_S = F_b \cos\theta \qquad \text{(Equation 4)}$$

$$F_b L \sin\theta = \tau_S + RF_S \qquad \text{(Equation 5)}$$

F_b = force on the bond

τ_S = shear stress

θ = the bond angle between the cell and the surface

L = lever arm (length)

CHAPTER 4: GPIBα-VWF WT-WT ROLLING INTERACTIONS UNDER SHEAR STRESS ARE REGULATED BY THE CATCH BOND MECHANISM WHILE OBSERVATIONS UNDER SHEAR STRESS REVEAL DIFFERENCES BETWEEN TYPE 2B AND 2M VWD

4.1 Introduction

As described in Chapter 1, activated platelets mediate the homeostatic response to vascular injuries. Evidence suggests clinical similarities in several bleeding disorders, yet differences in the bonding mechanics have been seen for interactions between the molecules involved in these disorders. In particular, the interactions between GPIbα and vWF are disrupted resulting in patient bleeding for type 2B VWD, type 2M VWD, and TTP.

In type 2B VWD it is believed that platelets form aggregates with the mutant vWF molecules in the bulk flow. Platelets become sequestered in these aggregates and are cleared from the blood resulting in mild thrombocytopenia and patient bleeding since the platelets are no longer available to interact at sites of vascular injury. Under normal conditions wt-wt catch-slip bond interactions likely prevent platelet aggregate formation by preventing increased adhesion between GPIbα and vWF at lower shear stresses [5].

In type 2M VWD there is decreased affinity between platelets and vWF molecules as defined by decreased ristocetin induced binding [6]. There is also evidence suggesting these mutations prevent a conformational change in the vWF molecule that would reveal the GPIbα binding site [7]. Additionally, there are increased off-rates and rolling

velocities for platelet-LOF vWF interactions. Further, AFM experiments show that LOF G561S vWF-A1 binding with GPIbα results in a catch bond, but at higher force [86]. However, the tether bond behavior of type 2M VWD-causing mutations under conditions of flow remains largely unknown.

To further investigate the mechanics of the tether bond, interactions were captured at 250 frames per second and a frame-by-frame analysis of these interactions was conducted. The steps in the binding of a single tether were analyzed and characterized in stages as either a stop or a go as has been described for selectin rolling interactions [17]. Here we analyze binding behavior to better understand how the changes seen in mutants associated with VWD occur at the tether bond level. Here it is shown that the rolling velocity and bonding behavior provide additional insight into how GPIbα and vWF regulate rolling, and it is shown for the first time that platelets rolling on G561S vWF-A1 molecules retain the catch-slip bond transition for rolling interactions under flow, which is consistent with AFM data by Auton et al. [86]. Further, it is shown by looking at the mean stop times, that under physiological fluid shear stress, the catch-slip transition for wt-GOF vWF-A1 interactions occurs at a lower shear stress than for wt-wt interactions, which occurs at a lower shear stress than for wt-LOF vWF-A1 interactions. Taken together, these data provide details of the GPIbα-vWF tether bond and the differences that exist between LOF and GOF mutations, and hence between type 2M and 2B VWDs.

Finally, changes in the GPIbα-vWF tether bond are investigated under conditions that mimic TTP. The experimental set up is similar to that for VWD diseases; however, platelet interactions are observed with whole vWF in either the presence or absence of ADAMTS-13. Using these techniques, it is seen that in the absence of ADAMTS-13

there are increased bond lifetimes, indicating that there are decreased off-rates. These data suggest a possible reason for aggregate formation with ultra large forms of vWF when ADAMTS-13 is absent, resulting in TTP.

4.2 Results

4.2.1 Rolling Velocities for Platelets Interacting with vWF Molecules

Platelet rolling velocities were calculated for interactions of platelets with wt vWF-A1 (Figure 4.1*A*), wt vWF-A1A2A3 (Figure 4.1*B*), or whole vWF (Figure 4.1*C*). The rolling velocity of platelets interacting with wt vWF-A1 first decreases and then increases with increasing shear stress (Figure 4.1*A*). Further, all wt vWF molecules display a catch-slip transition with rolling velocity first decreasing at lower shear stresses, followed by transitioning to increasing velocities at higher shear stresses. Minimum rolling velocities were similar for all wt vWF molecules (Figure 4.1). The catch-slip transition occurs for wt vWF-A1 (Figure 4.1*A*) and whole vWF (Figure 4.1*C*) at 16 dyn/cm^2, while the transition for wt vWF A1A2A3 (Figure 4.1*B*) occurs at 8 dyn/cm^2.

4.2.2 Rolling Velocities on wt vWF-A1 Domain with Different Fluid Viscosities

In Figure 4.2, purified platelet rich plasma with or without 6% Ficoll was perfused across a wt vWF-A1 coated coverslip (100 μg/mL) at 37^{o}C. Results were plotted against both shear rate (Figure 4.2*A*) and shear stress (Figure 4.2*B*). There is an increase in shear stress by a factor of 1.8 at a given shear rate for samples containing 6% Ficoll. When plotted against shear rate the curves do not align (Figure 4.2*A*).

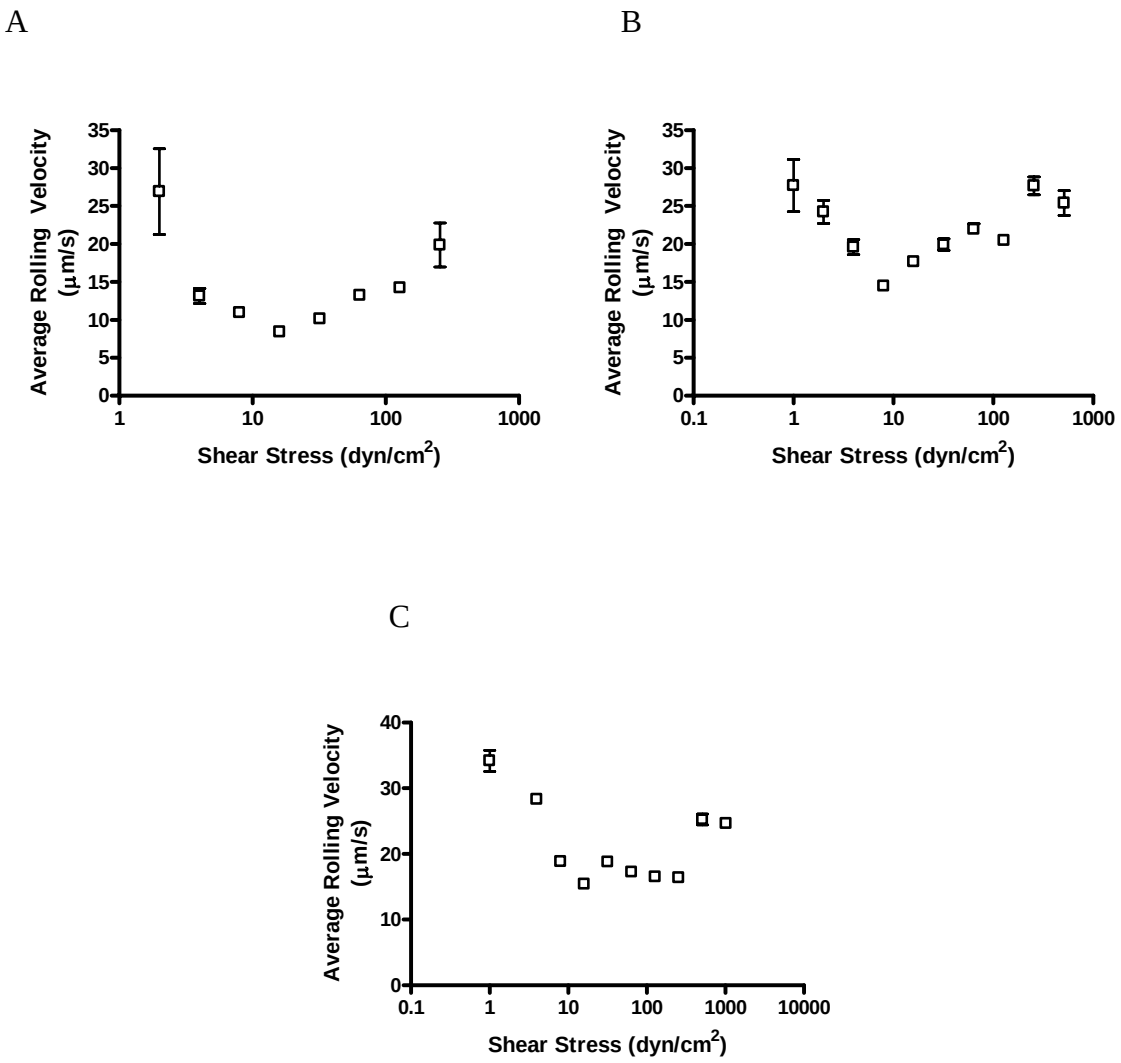

Figure 4.1: Rolling velocity of platelets on various forms of wild-type vWF molecule: (A) wt vWF-A1 (n = 14 to 256), (B) wt vWF-A1A2A3 (n = 10 to 36), or (C) wt whole vWF (n = 44 to 277). Data represent mean ± SEM. Each catch-slip transition is statistically significant with a p-value < 0.05.

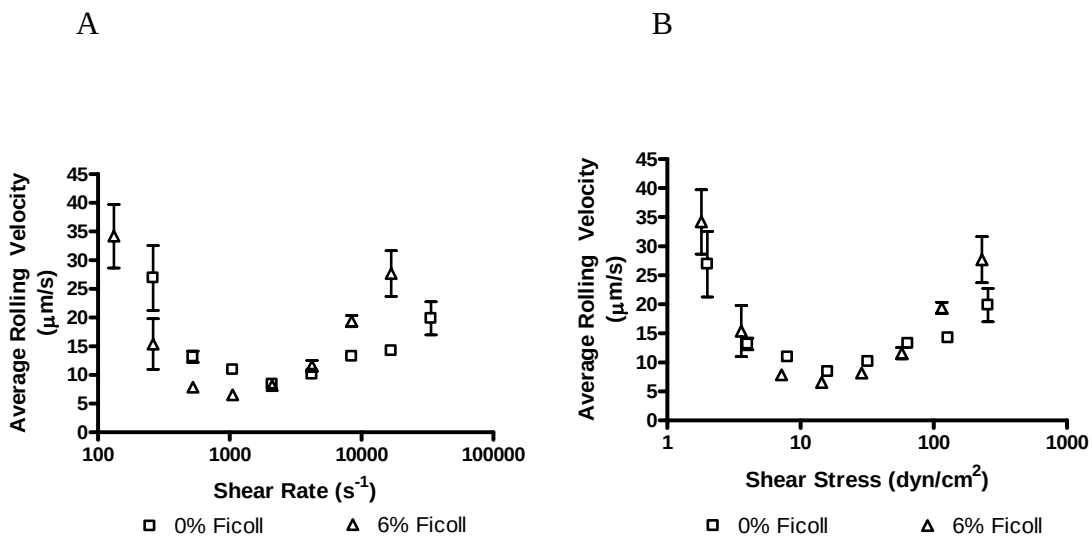

Figure 4.2: Effects of viscosity on rolling velocity of wt vWF-A1 molecules for (A) shear rate and (B) shear stress for platelets rolling on wt vWF-A1. Data represent the mean ± SEM. For 0% Ficoll n = 14 to 256 cells and for 6% Ficoll n = 10 to 112 cells. Each catch-slip transition is statistically significant with a p-value < 0.05.

When rolling velocities were plotted as a function of shear stress, the curves align (Figure 4.2*B*). These results show that rolling interactions depend on the shear stress applied to the bond. Therefore, this data suggests that the bonding mechanism is force, rather than transport, dependent, suggesting that bond force governs rolling velocity interactions.

4.2.3 Effects of Viscosity on Mean Stop Times for Platelets Rolling on wt vWF-A1

In Figure 4.3, purified platelet rich plasma with or without 6% Ficoll was perfused across a wt vWF-A1 coated coverslip (100 μg/mL). Mean stop times were plotted against both shear rate (Figure 4.3*A*) and shear stress (Figure 4.3*B*). Shear stress is increased by a factor of 1.8 at a given shear rate by the addition to the samples of 6% Ficoll.

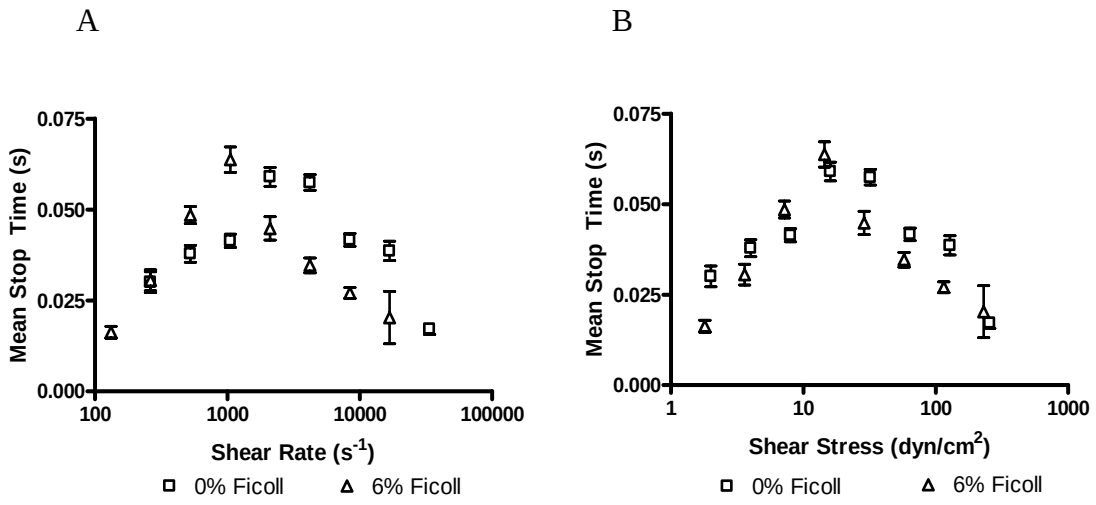

Figure 4.3: Effects of viscosity on mean stop times of wt vWF-A1 molecules: (A) shear rate and (B) shear stress for platelets rolling on wt vWF-A1. Data represent the mean ± SEM. For 0% Ficoll n = 14 to 256 cells and for 6% Ficoll n = 10 to 112 cells. Each catch-slip transition is statistically significant with a p-value < 0.05.

The curves do not align when plotted against shear rate (Figure 4.3*A*), but do align when plotted as a function of shear stress (Figure 4.3*B*). Together these data suggest a force rather than transport dependent bonding mechanism. Alignment with shear stress suggests bond force governs mean stop time interactions.

4.2.4 Effects of Shear Stress on Mean Stop Time and Mean Go Time for Platelets Rolling on wt vWF-A1 Molecules

Purified platelet rich plasma with or without 6% Ficoll was perfused across a wt vWF-A1 coated coverslip (100 μg/mL) at 37^{o}C. The average amount of time a cell spent in either the stop or the go phase over a one second interval was calculated from rolling data. Figure 4.4 shows that mean go time is constant when compared to mean stop times.

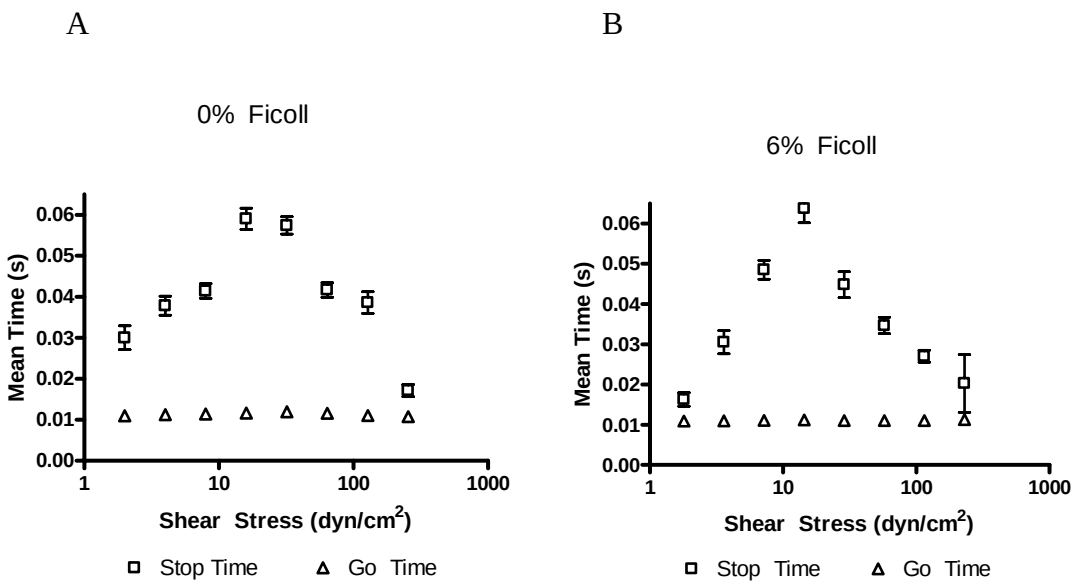

Figure 4.4: Comparison of mean stop and go times for platelet rolling interactions with wt vWF-A1 molecule: (A) 0% Ficoll (n = 14 to 256) and (B) 6% Ficoll (n = 10 to 112). Data represent the mean ± SEM. Each catch-slip transition is statistically significant with a p-value < 0.05.

Furthermore, the mean go time is less than the mean stop time for all shear stresses investigated. These data indicate that the mean go time is unaffected by the shear stress. Further, because the biphasic mean stop time has longer durations, the data suggests that the mean stop time is a controlling parameter for rolling interactions.

4.2.5 Transient Tethering Lifetime Measurements for Platelets Rolling on wt vWF-A1 Molecule

Off-rates were calculated for platelet interactions with wt vWF-A1 molecule. Platelets rich plasma was perfused across low density vWF-A1 molecule. The time a platelet spent stopped was measured. A plot of the ln (# cells bound) versus time bound was used to calculate the off-rate for each shear stress as described in the Methods section 3.14. In Figure 4.5 the off-rate first decreases, then increases with increasing shear stress. This data shows the bonds dissociate more rapidly at the lowest shear

stresses, less rapidly as shear stress is increased, and then the bonds dissociate more rapidly with increasing shear stress.

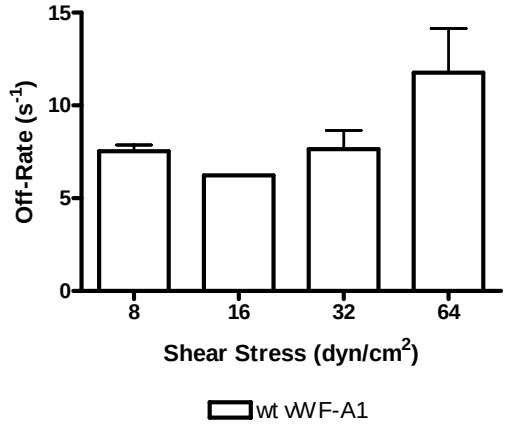

Figure 4.5: Transient tethering of platelets on wt vWF-A1 molecule. Data represent mean ± SEM and n = 2 experiments (40 to 94 cells per experiment), except for 16 dyn/cm^2 which represents 1 experiment (104 cells per experiment).

This trend indicates a catch-slip transition for the off-rate between platelets and wt vWF-A1 molecules. The relationship here is reciprocal compared to the rolling velocity data seen in Figure 4.1*A*. Because off-rate is a force dependent parameter, this data also suggests that the rolling interactions between platelets and wt vWF-A1 are force dependent.

4.2.6 Rolling Velocities of Platelets Interacting with vWF Molecules Containing Mutations

Platelet rolling velocities were calculated for interactions of platelets with GOF R687E vWF-A1 (Figure 4.6*A*) and LOF G561S vWF-A1 (Figure 4.6*B*).

A B

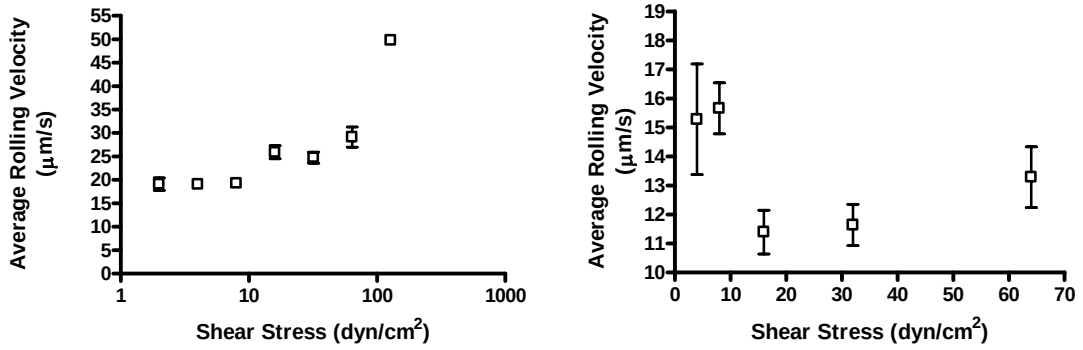

Figure 4.6: Rolling velocity of platelets on mutant vWF molecules: (A) GOF R687E vWF-A1 (n = 5 to 121) and (B) LOF G561S vWF-A1 (n = 23 to 98). Note that because there is decreased association between platelets and LOF G561S vWF-A1 (B), fewer interactions occur at all shear stresses and none occur at the highest shear stresses measured for other vWF molecules. Data represent mean ± SEM. Each catch-slip transition is statistically significant with a p-value < 0.05.

Unlike wt vWF molecules (Figure 4.1) and LOF G561S vWF-A1 (Figure 4.6*B*), all of which display a catch-slip transition with rolling velocity first decreasing at lower shear stresses, then transitioning to increasing velocities at higher shear stresses, GOF R687E vWF-A1 (Figure 4.6*A*) displays only a slip bond. Further, minimum rolling velocities were similar for LOF G561S vWF-A1 (Figure 4.6*B*) compared to all wt vWF molecules (Figure 4.1).

4.2.7 The Mean Stop Time Catch-Slip Transition Shear Stress Varies Depending on the vWF-A1 Molecule

Interactions of platelets rolling on vWF-A1 molecules were characterized frame-by-frame as stop or go motions, and rolling interactions were measured at 250 fps. Figure 4.7 shows the mean stop time data, which is the average time a cell spends in the stop phase during a one second interval.

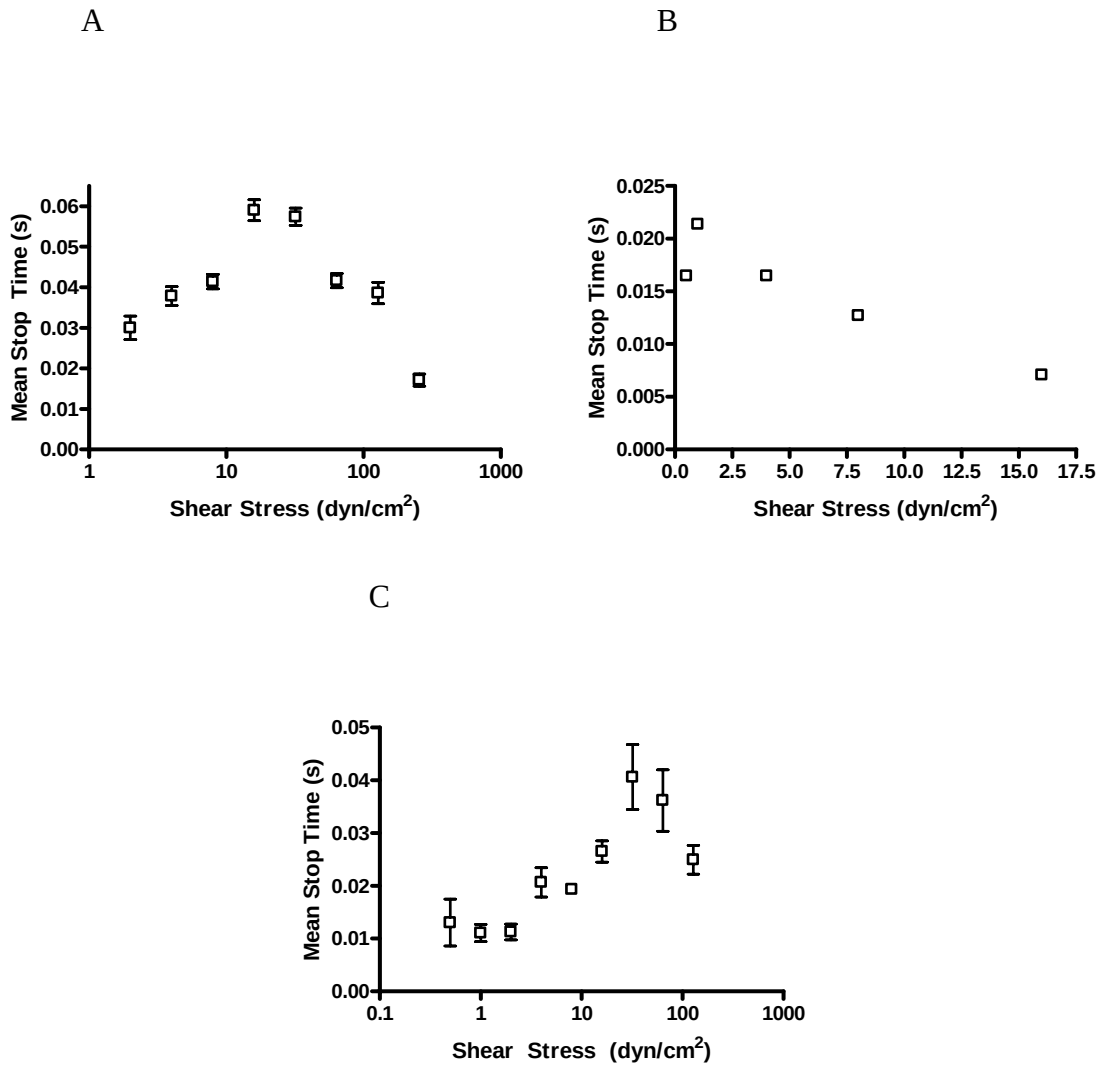

Figure 4.7: Mean stop times of platelets on vWF-A1 molecules: (A) wt vWF-A1 (n = 14 to 256), (B) GOF R687E vWF-A1 (n = 5 to 104), and (C) LOF G561S vWF-A1 (n = 11 to 382). Data represent the mean ± SEM. Each catch-slip transition is statistically significant with a p-value < 0.05.

For all vWF-A1 molecules, the mean stop time first increases, then decreases as the shear stress increases. The catch-slip transition for GOF R687E vWF-A1 (2 dyn/cm^2, Figure 4.7*B*) is decreased compared to that of wt vWF-A1 (16 dyn/cm^2, Figure 4.7*A*). However, this transition for LOF G561S vWF-A1 (32 dyn/cm^2, Figure 4.7*C*) is increased compared to that of wt vWF-A1 molecule (16 dyn/cm^2, Figure 4.7*A*).

4.2.8 Transient Tethering Lifetimes for Platelets Interacting with LOF G561S vWF-A1

Off-rates were calculated for platelet interactions with LOF G561S vWF-A1 molecule (Figure 4.8). Platelet rich plasma was perfused across low density vWF-A1 molecule. The time a platelet spent stopped was measured.

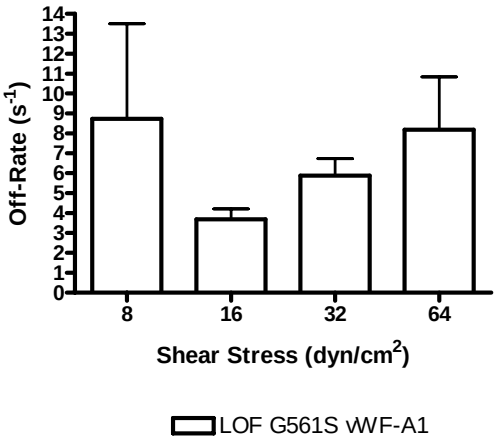

Figure 4.8: Transient tethering of platelets on LOF G561S vWF-A1 molecule. Data represent mean ± SEM and n = 7 experiments (2 to 89 cells per experiment), except for 8 dyn/cm2, which represents 5 experiments (3 to 30 cells per experiment).

A plot of the ln (# cells bound) versus time bound was used to calculate the off-rate for each shear stress as described in the Methods section 3.14. In Figure 4.8 the off-rate first decreases, then increases with increasing shear stress. This data shows that the bonds dissociate more rapidly at the lowest shear stress, less rapidly as shear stress is increased, and then the bonds dissociate more rapidly with increasing shear stress. This trend indicates a catch-slip transition for the off-rate between platelets and LOF G561S vWF-A1 molecules similar to that seen for platelets and wt vWF-A1 molecules. The relationship here is reciprocal compared to the rolling velocity data seen in Figure 4.6*B*.

Because off-rate is a force dependent parameter, this data also suggests that the rolling interactions between platelets and LOF G561S vWF-A1 are force dependent.

4.2.9 Tether Rate Analysis for Platelets Interacting with wt or LOF G561S vWF-A1

In Figure 4.9 the role of on-rate in the GPIbα-vWF tether bond formation was investigated. Platelets were perfused across a vWF-A1 coated surface. Here the initial tethering of cells was observed and quantified as percentage of cells tethered (Figure 4.9*A*) and as number of cells tethered per minute (Figure 4.9*B*). These data sets are preliminary and represent one or two experiments as noted in Figure 4.9. Here the percentage of tethered cells is low for both platelet interactions with wt vWF-A1 and LOF G561S vWF-A1 at lowest shear stresses (Figure 4.9*A*).

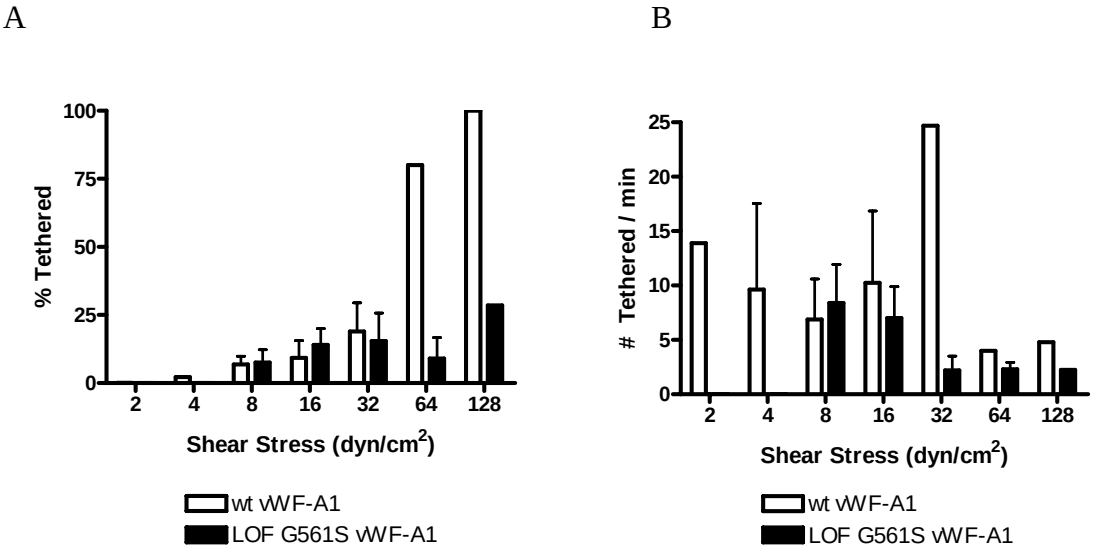

Figure 4.9: Tethering frequency of platelet interactions with wt vWF-A1 and LOF G561S vWF-A1 molecules. Percentage of platelets tethering to wt or LOF G561S vWF-A1 molecules (A) and the number of platelets tethering to wt or LOF G561S vWF-A1 molecules per minute (B). Data represent mean ± SEM and n = 2 experiments, except for LOF G561S vWF-A1 data at 128 dyn/cm^2 and wt vWF-A1 data at 2, 32, 64, and 128 dyn/cm^2, where n = 1 experiment.

However, at the highest shear stresses studied, the percentage tethered for platelet interactions with wt vWF-A1 is greater than that for platelet interactions with LOF G561S vWF-A1 (Figure 4.9*A*). The number of platelets tethering per minute is similar for wt vWF-A1 and LOF vWF-A1 (Figure 4.9*B*), and is increased at the lower shear stresses and decreased at the higher shear stresses studied. These data suggest a reason why LOF G561S vWF-A1 interactions may have decreased affinity binding compared to wt vWF-A1.

4.2.10 Effect of the Presence of ADAMTS-13 Enzyme on Platelet Interactions with Whole vWF

Platelets were perfused across a low density whole vWF coated surface that either was or was not exposed to the enzyme ADAMTS-13. The transient tethering lifetimes were measured for each shear stress and used to calculate the bond lifetimes (Figure 4.10) as described in Methods section 3.14. Data show that in both the presence (Figure 4.10, open triangles) and the absence of ADAMTS-13 (Figure 4.10, open squares) the bond lifetime is biphasic, suggesting that there is a catch-slip transition for both cases. Further, at lower shear stresses studied the bond lifetimes in the presence of ADAMTS-13 (Figure 4.10, open triangles) are decreased compared to bond lifetimes calculate in the absence of ADAMTS-13 (Figure 4.10, open squares). These data indicate that when the ADAMTS-13 enzyme is present, the off-rate for the GPIbα-vWF interaction is increased.

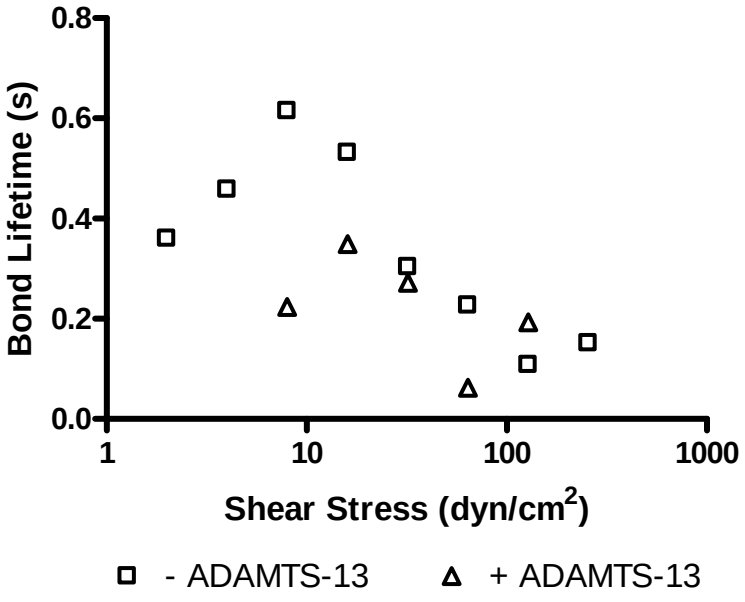

Figure 4.10: Effect of the presence of ADAMTS-13 on bond lifetime for platelets interacting with whole vWF. Data represent mean ± SEM and n = 1 experiment with 6 to 115 cells per shear stress.

4.3 Discussion

Analyzing interactions between GPIbα and vWF molecules shows differences between wt vWF molecules and vWF molecules with mutations causing type 2M and 2B von Willebrand Diseases. The type 2M mutation used in these studies, G561S, occurs naturally, and is characterized by decreased platelet binding in the presence of ristocetin (LOF), as well as by a normal multimer pattern and normal number of vWF antigens present [6]. The type 2B mutation used in these studies, R687E, is a non-naturally occurring mutation with characteristics similar to those seen for naturally occurring type 2B mutations and is characterized by enhanced platelet binding with ristocetin (GOF) [12, 13].

Here we show that platelets interacting with wt vWF molecules display biphasic rolling velocity, mean stop time, and off-rate profiles (Figures 4.1 through 4.8). Platelets rolling on wt molecules have rolling velocities that first decrease, then increase with increasing shear stress (Figure 4.1). This trend suggests that as the platelets are rolling more slowly, the bond is lasting for a longer time, a trend indicative of a catch bond. Then, as shear stress is further increased, the rolling velocity increases with increasing shear stress, suggesting that the bond is lasting for increasingly shorter times, a trend indicative of a slip bond. Such catch-slip transitions have been previously shown in two other biological systems. Flow enhanced adhesion was shown for both interactions of selectins with their respective ligands [17, 18, 78], and interactions between bacterial FimH and mannose residues on glycoproteins [72, 87].

We extend the rolling interactions to observe more detailed motions of the platelets rolling on vWF molecules. First, to further investigate these rolling interactions, the mean stop time for platelets interacting with wt vWF-A1 was measured (Figure 4.7). Rolling parameters were calculated from frame-by-frame rolling velocity data collected at 250 fps. To quantify these interactions each frame is characterized as a stop or a go motion based on whether the cell is accelerating or decelerating in each frame relative to the previous frame as described in Methods section 3.13. These values are reported here as mean stop times and mean go times. Though this type of data does not directly measure single bond behavior, it can be used to infer information about bond lifetimes of molecules interacting under fluid forces. For platelet-wt vWF-A1 interactions we show that the mean stop time first increases and then decreases with increasing shear stress (Figure 4.7*A*). Because mean stop time indicates the amount of time a cell spends

stopped, it is analogous to the bond lifetime. Therefore, in terms of bond lifetime, this data suggest that the bond lifetime is increasing at lower shear stresses with increasing shear stress, while it is decreasing as the shear stress is further increased beyond a maximum lifetime. This trend likely indicates regions of catch bonding followed by regions of slip bonding as shear stress is increased. Further, L-selectin coated microspheres rolling on a PSGL-1 surface show a similar trend [17].

We also studied the mean go times for wt-wt rolling interactions, which represent the average amount of time the platelets spent moving forward after a stop. Based on the model used [17], the mean go time is the combination of the cell first pivoting forward after the previous bond is broken and the cell stretching the new trailing bond as it moves forward. Thus, the observations made here can be used to infer information about the rate of association for the tether bond. The rolling step interactions show that the mean go time for wt-wt interactions is constant when compared to the mean stop time for wt-wt interactions (Figure 4.4). Further, the data shows that the mean go time is less than the mean stop time for all shear stresses. Together this data suggest that the mean stop time is more responsive than go time for GPIbα-vWF tether bond interactions and is likely the controlling parameter in GPIbα-vWF rolling interactions. Because the stop time suggests information about how long a bond lasts (bond lifetime), and go time suggests information about how bonds are formed, together these data suggest that the bond lifetime regulates wt-wt interactions subjected to fluid shear stress. Since the mean go time is constant relative to the mean stop time, these data suggest that the time spent by the cell moving forward would be unaffected by changes in fluid shear stress when compared to changes in the time the cell spends stopped. Further, because the mean stop

time suggests changes in the bond lifetime (regulated by force) regulate wt-wt interactions, these observations can be extended to suggest that a force mechanism, rather than a transport mechanism, regulates the GPIbα-vWF tether bond when subjected to fluid shear stress.

To study the bond lifetime more directly, the transient tethering lifetime for platelets interacting with either wt or LOF G561S vWF-A1 was measured under conditions of force applied by fluid forces in a parallel plate flow chamber (Figures 4.5 and 4.8). The bond lifetime is calculated from the dissociation rate, or off-rate (k_{off}), for the bond, which is inversely proportional to the bond lifetime. Figures 4.5 ad 4.8 both show a decrease in the dissociation rate as shear stress is increased to a minimum value after which the dissociation rate increases with further increasing shear stress. These data are consistent with data published by us and our collaborators [5, 86].

For platelet interactions with wt vWF-A1, we show for mean stop times that increasing the viscosity (and force) at a given shear rate, results in curves that align when plotted versus shear stress, but do not align when plotted versus shear rate (Figure 4.3). These data are consistent with the rolling velocity data presented here (Figure 4.2) and previously by us and our colleagues [5], where, when the viscosity is increased for wt-wt interactions, the data also aligns when plotted against shear stress, but not shear rate. The mean stop time indicates the average amount of time during a one second interval that the cell spends stopped. This parameter can be used to infer information about bond lifetime and off-rate because this type of measurement is an indicator for how long the bond is stopped before the platelet moves again. The data, therefore, suggests that the bond lifetime of wt-wt interactions increases then decreases with increasing applied force.

Further, these data suggest that the off-rate decreases (enhanced bonding), then increases (decreased bonding) as force is increased. These data show that the catch-slip transition seen for rolling velocity describes a more specific property of the bonding mechanism. Further, these data show that not only are the overall rolling interactions governed by force, but that more specific interactions (the mean stop time in this case) are also governed by force.

The combination of rolling velocity, mean stop time, off-rate, and viscosity data indicates that the bond for wt-wt interactions is regulated by force mechanisms. To add further evidence in support of force dependent platelet interactions with wt vWF molecules being regulated by a catch-slip transition, our colleagues conducted single molecule studies using AFM to determine bond lifetimes and used MD simulations to observe possible structural changes from the binding between GPIbα and vWF-A1 under applied force [5].

To study differences in the tether bond, we first observed rolling velocities for three wt vWF molecules: vWF-A1 (Figure 4.1*A*), vWF-A1A2A3 (Figure 4.1*B*), and whole vWF (Figure 4.1*C*). Following wt vWF molecule studies, we studied changes using GOF R687E vWF-A1 (Figure 4.6*A*) and LOF G561S vWF-A1 (Figure 4.6*B*). In both cases the rolling velocity of platelets interacting with the vWF molecule first decreased and then increased with increasing shear stress, with the exception of interactions with GOF R687E vWF-A1, which showed only increasing velocity with increasing shear stress.

For whole vWF the rolling velocity did not increase as dramatically as was seen for both wt vWF-A1 and wt vWF-A1A2A3 studies. This result is possibly due to the

presence of the RGD sequence found in the whole vWF molecule, but that is omitted in the other molecules studied. It is likely that the RGD sequence binds integrins that were present on the platelet surface. Because platelets were treated with prostaglandin E-1 and citrate buffer, they did not activate significantly. It is possible, however, that some integrins were activated at these higher shear stresses, which would cause the platelets to move more slowly due to formation of some longer lasting bonds, but not enough to result in complete platelet arrest.

The minimum rolling velocity for platelets interacting with whole vWF molecules occurred at 16 dyn/cm^2, which is the same minimum observed for both wt vWF-A1 and LOF G561S vWF-A1 surfaces (Figures 4.1*A* and 4.6*B*, respectively). Interestingly, the minimum observed for platelet interactions with wt vWF-A1A2A3 occurred at a shear stress of 8 dyn/cm^2 (Figure 4.1*B*). Previously, it has been suggested that a decrease in the catch-slip transition force indicates a destabilization of the vWF molecule used [86]. Therefore, the transition occurring at a lower shear stress for wt-A1A2A3 vWF molecule could suggest that this configuration of the vWF molecule may be less stable than its wt counterparts.

We have shown that biphasic catch-slip bonds govern wt-wt interactions (here and in [5]), which shows that this bond is force dependent, and, therefore that force plays an important role in the bonding behavior between GPIbα and vWF molecules. However, the same mechanism was not seen for wt GPIbα-type 2B VWD interactions, in which the catch bond behavior was absent [5]. Similar results have been reported for interactions for selectins bearing single mutations in either the hinge region between lectin and EGF domains in L-selectin [68] or on the ligand binding surface of the L-

selectin molecule [69]. For these molecule pairs, the mutations in the hinge region reduced the bond lifetimes at low forces and reduced the shear threshold [68], while mutations in the L-selectin binding site surface eliminated the shear threshold [69].

Further, we show the novel observation that platelet-LOF interactions under fluid forces retain the catch-slip transition when subjected to fluid shear stress (Figures 4.7*B* and 4.7*C*), but this transition occurs at a different shear stress than seen in wt-wt interactions (Figure 4.7). Our data show that at physiological temperatures, GOF and LOF mutations each differ from wt vWF-A1, but in unique ways (Figures 4.1, 4.6, and 4.7). These data together suggest that although the clinical observation for VWD diseases 2M and 2B are similar, the mechanism for the tether bond dissociation is different.

To further study the changes introduced by mutations in vWF, the mean stop times for each vWF-A1 molecule were calculated and compared. Here we report that as shear stress is increased, the mean stop time increases, then decreases, for each type of vWF-A1 molecule studied reflecting the catch-slip transition seen in the rolling velocity data for wt-wt interactions (Figure 4.1*A*). For wt-wt interactions at 37^{o}C both the rolling velocity and the mean stop time data catch-slip transitions occur at 16 dyn/cm^2 (Figures 4.1*A* and 4.3*A*), which is similar to the rolling velocity transition shear stress we and colleagues reported for wt-wt interactions at room temperature [5]. Further, the catch-slip transition seen in mean stop times is present for all types of vWF-A1 molecules. Mean stop time data suggests how the off-rate or bond lifetime for each interaction is modulated. Our data shows that the transition force for LOF G561S vWF-A1 is greater than that for wt vWF-A1, which is greater than that for GOF R687E vWF-A1 (Figure

4.7). These data suggest that greater force is required for maximum bond lifetime for LOF G561S vWF-A1 compared to wt vWF-A1, while less force is required for GOF R687E vWF-A1 compared to wt vWF-A1.

Recently, Auton et al. [86] studied the thermodynamic stability of vWF-A1 wt and mutant molecules. They showed for single molecule AFM data that the catch-slip transition for bond lifetimes also existed for both types of mutants and wt vWF-A1. Further, their AFM data and thermodynamic data show that the transition for GOF mutations in vWF-A1 occurs at lower forces than seen for wt vWF-A1, which occurs at lower forces than for LOF mutations in vWF-A1. The mean stop time data shown here (Figure 4.3) suggest that the thermodynamic data presented by Auton et al. [86] are consistent with GPIbα-vWF interactions under physiological flow conditions.

To gain a better understanding of the bonding behavior of LOF vWF-A1 mutations compared to wt vWF-A1 molecules, we studied on-rate indicators by measuring and quantifying tethering frequency (Figure 4.9). Here we calculate the percentage of cells tethered in one minute (Figure 4.9*A*) and the number of cells that tethered per minute (Figure 4.9*B*). The percentage of first time platelet tethers for interactions with wt vWF-A1 and LOF G561S vWF-A1 were similar at lower shear stresses, but the percent tethered was greater for wt vWF-A1 compared to LOF G561S vWF-A1 at higher shear stresses (Figure 4.9*A*). The number of cells tethering was similar for both wt and LOF G561S vWF-A1 molecules (Figure 4.9*B*). Because the number of tethers per minute was similar, but the percent tethered was greater for wt vWF-A1 compared to LOF G561S vWF-A1 at higher shear stresses, this data suggests that the wt vWF-A1 molecule has more successful interactions with platelets. Because

the percent of platelets tethered and the number of tethers per minute are determine by observing first time tethers, these data suggest information about the on-rate. At the lower shear stresses both the percent tethered and the number tethering per minute are similar, suggesting that the on-rate for these two vWF-A1 molecules is similar at these shear stresses. Together with the changes seen in mean stop time (Figure 4.7) and force dependency (Figures 4.2 and 4.3) data shown earlier, this data provides further evidence that changes in the GPIbα-vWF tether bond are force and not transport dependent.

Further, in Figures 4.7 *A* and *B*, we saw that the mean stop time maximum for LOF G561S vWF-A1 (Figure 4.7*B*) was shifted to a higher shear stress when compared to wt vWF-A1 (Figure 4.7*A*). Together, these data indicate that at the shear stress where the LOF mutant becomes conformationally active, there are few successful tethers, which would result in fewer opportunities for GPIbα-vWF interactions. The decreased number of interactions could explain why patients with type 2M VWD bleed.

The rolling velocity of platelets interacting with different vWF surfaces was measured at 37^{o}C and 250 frames per second. We show that all wt-wt interactions and wt-LOF interactions contain a catch-slip transition, while wt-GOF interactions have only slip bond behavior. Further the effects of a change in force, by changing the viscosity, were observed for rolling velocities and mean stop times. Mean stop and go time data showed differences between the different vWF-A1 molecules and that for wt-wt interactions the mean stop time dominated the rolling interactions when comparing mean stop and go times. Transient tethering lifetime and first time tethering measurements give insight into the kinetics of the GPIbα-vWF tether bond.

These observations, over a range of shear stresses, reveal the presence of catch-slip transitions at shear stresses that may reflect changes in vWF structure not only for wt-wt interactions, but also for wt-LOF vWF-A1 (rolling and mean stop time data) and wt-GOF vWF-A1 (mean stop time data) interactions. Additional studies will lead to a greater understanding of how naturally occurring mutations in vWF result in each type of VWD studied. The data shown here provides details of the GPIbα -vWF tether bond and show differences that exist between different types of mutations in the vWF molecule, and hence between type 2M and type 2B VWDs. Here the data provide insight into a possible reason bleeding is seen for both GOF and LOF mutations in vWF. For GOF type 2B VWD, there are likely prolonged lifetimes for platelet interactions with GOF R687E vWF-A1 at the lowest shear stresses studies, which result in platelet binding to soluble vWF, effectively clearing platelets from the bulk fluid, so there are not enough to interact at sites of vascular injury. For LOF type 2M VWD mutations, there is decreased adhesion between platelets and LOF vWF mutants. Because the catch-slip transition, where bonds last for the longest time, is at higher shear stress, and the likelihood of a successful tethering event is decreased at these shear stresses, it is likely that fewer successful GPIbα-vWF interactions occur when the LOF mutations in vWF are present. Together these observations suggest that bleeding may occur for type 2M mutants because the shear stress where these mutants are most likely to successfully bind platelets are too high to allow for enough cells to be available at the sites of injury. Determination of the biomechanical and kinetic functions of wt and mutant molecules has helped us elucidate the possible physiological mechanisms inherent in interactions between GPIbα

and vWF leading to a better understanding of both type 2B and type 2M VWD bleeding disorders.

Finally, we conducted preliminary studies to characterize the effect of the presence of the protease ADAMTS-13. Defects in ADAMTS-13 result in thrombus formation and are a cause of TTP, which also results in patient bleeding [65]. Here we study the bond lifetime of GPIbα-vWF interactions in the presence and absence of ADAMTS-13 (Figure 4.10). At shear stresses lower than 32 dyn/cm^2, the bond lifetimes for interaction in the absence of ADAMTS-13 (Figure 4.10, open squares) are greater than the bond lifetimes for interaction in the presence of ADAMTS-13 (Figure 4.10, open triangles). Above, and including 32 dyn/cm^2, the bond lifetimes either follow the same trend or are similar (32 dyn/cm^2 and 64 dyn/cm^2). These data indicate that at most shear stresses and at all lower shear stresses the presence of ADAMTS-13 decreases the bond lifetime, which increases the off-rate. Therefore, the presence of the enzyme enhances bond dissociation. These data agree with the observation that when ADAMTS-13 is present thrombus formation is prevented at sites of vascular injury. When the enzyme is absent the bond lifetime is increased, which is in agreement with aggregate formation seen when ADAMTS-13 is defective or missing [65]. These data begin to offer an explanation for thrombus formation seen in TTP patients.

Overall, the data presented in this chapter provides evidence to explain the bonding mechanism underlying three vWF bleeding disorders: type 2B VWD, type 2M VWD, and TTP. Further, this bonding data offer possible explanations of why patients bleed with each of these differently presenting diseases.

CHAPTER 5: OBSERVATIONS UNDER SHEAR STRESS REVEAL DIFFERENCES FOR INTERACTIONS BETWEEN WT AND GOF K237V GPIBα INTERACTING WITH WT VWF-A1

5.1 Introduction

In Chapter 4, we saw that mutations in vWF molecules resulting in type 2B or type 2M VWD change the bonding behavior between GPIbα and vWF. Now in Chapter 5, we study mutations found in the GPIbα molecule rather than the vWF molecule. As with VWD mutations, pt-VWD mutations may lead to abnormal interactions between GPIbα and vWF resulting in mild to moderate bleeding. These GOF mutations in the GPIbα molecule have enhanced adhesion of the GPIbα receptor resulting in clearance of hemostatically active large vWF multimers from the blood plasma [88]. Two naturally occurring mutations are G233V [89] and M239V [90], both of which are valine substitutions. Additional valine substitutions have previously been screened and studied [91]. Our lab has previously shown that the GOF mutation K237V mutation showed the most dramatic decrease in rolling velocity compared to wt GPIbα [91]. For this reason, the K237V mutation was selected to represent GOF GPIbα mutations in these studies. GOF mutations in GPIbα have kinetics similar to those seen for the GOF mutations in the vWF molecule [8]. Further, it has been suggested that changes in rolling velocities at shear stresses higher than those studied here indicate that kinetics play an important role

in modulating the binding between GPIbα and vWF [16]. The kinetics of GPIbα-vWF interactions have previously been studied by several groups and it has been seen that there are rapid interactions between GPIbα and vWF [21-23, 27]. Based on these observations there is no consensus on whether on-rate or off-rate regulates rolling for wt and GOF GPIbα interactions, though our lab previously observed that both on-rate and off-rate may regulate rolling interactions [16].

To further investigate the mechanics of the tether bond, interactions were captured at 250 frames per second and a frame-by-frame analysis of these interactions was conducted. The stages in bonding of a single tether were analyzed [17] and characterized in stages as either a stop or a go as described in Methods section 3.13. Here we analyze binding behavior to better understand how the changes seen in mutants associated with pt-VWD occur at the tether bond level. We show that the rolling velocity and bonding behavior provide additional insight into how GPIbα and vWF regulate rolling, and show for the first time that CHO cells expressing GOF K237V GPIbα rolling on wt vWF-A1 molecules may be regulated by transport rather than force mechanisms. Taken together, these data provide details of the GPIbα-vWF tether bond and the differences that exist between wt and GOF mutations in GPIbα.

5.2 Results

5.2.1 Rolling Velocities for CHO Cells Expressing wt GPIbα Interacting with wt vWF-A1

The rolling velocities of CHO cells expressing wt GPIbα were calculated for interactions with wt vWF-A1. The rolling velocity first decreases and then increases with increasing

shear stress (Figure 5.1), with a transition shear stress at 0.08 dynes/cm^2. Because CHO cells are much larger than platelets (~14 μm versus ~1.5 μm in diameter, respectively), to compare this data to the platelet data from Chapter 4 the force on the bond at the transition shear stresses was determined as described in Methods section 3.15, and are shown here in Table 5.1. As seen in Table 5.1, the force on the bond for CHO cells expressing wt GPIbα rolling on wt vWF-A1 is similar to that for platelets rolling on wt vWF-A1A2A3.

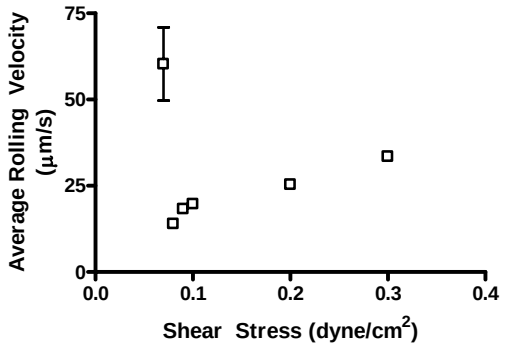

Figure 5.1: Rolling velocities of CHO cells expressing wt GPIbα interacting with wt vWF-A1. Data represent mean ± SEM and n = 3 to 33 cells.

Table 5.1: Comparison of minimum force for wt-wt interactions

Cell Type	Surface	Shear Stress (dyn/cm^2)	Force (pN)
Platelets	wt vWF-A1	16	58
CHO cells expressing wt GPIbα	wt vWF-A1	0.08	28
Platelets	wt vWF-A1A2A3	8	28

5.2.2 Rolling Velocities for CHO Cells Expressing GOF K237V GPIbα Interacting with wt vWF-A1

The rolling velocities of CHO cells expressing GOF K237V GPIbα were calculated for interactions with wt vWF-A1. The rolling velocity only increases with increasing shear stress (Figure 5.2) indicating that the catch bond seen for wt-wt interactions is lost for this mutant.

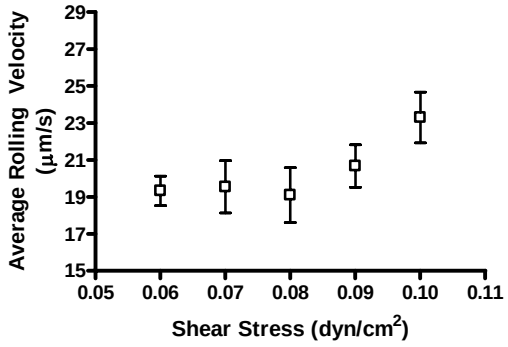

Figure 5.2: Rolling velocities of CHO cells expressing GOF K237V GPIbα interacting with wt vWF-A1. Data represent mean ± SEM and n = 41 to 134 cells.

5.2.3 Mean Stop Time for CHO Cells Expressing wt GPIbα Versus GOF K237V GPIbα Interacting with wt vWF-A1

Mean stop time for CHO cells expressing wt GPIbα rolling on wt vWF-A1 (Figure 5.3, open squares) first increases, then decreases, as shear stress is increased.

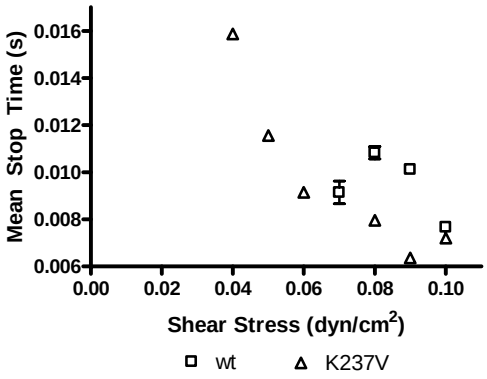

Figure 5.3: Mean stop times of CHO cells expressing wt or GOF K237V GPIbα interacting with wt vWF-A1. Data represent mean ± SEM and n = 3 to 22 cells.

Mean stop time for CHO cells expressing GOF K237V GPIbα rolling on wt vWF-A1 (Figure 5.3, open triangles) only decreases with increasing shear stress. Further, at lowest shear stresses the mean stop time for GPIbα carrying the GOF mutation is greater than those for wt GPIbα, suggesting that the bonds for GPIbα which carry the GOF mutation last longer than those for wt GPIbα. Because the mean stop time is larger for the GOF mutant at lowest shear stress compared to wt GPIbα, these data suggest an explanation of why aggregates form when GOF mutations are present. When the molecule pair comes together the bonds last longer for GPIbα molecules carrying a GOF mutation.

5.2.4 Effects of Viscosity on Rolling Velocity for CHO Cells Expressing wt GPIbα Interacting with wt vWF-A1

In Figure 5.4 CHO cells expressing wt GPIbα were perfused across wt vWF-A1 (open triangles) with and without (open squares) 6% Ficoll.

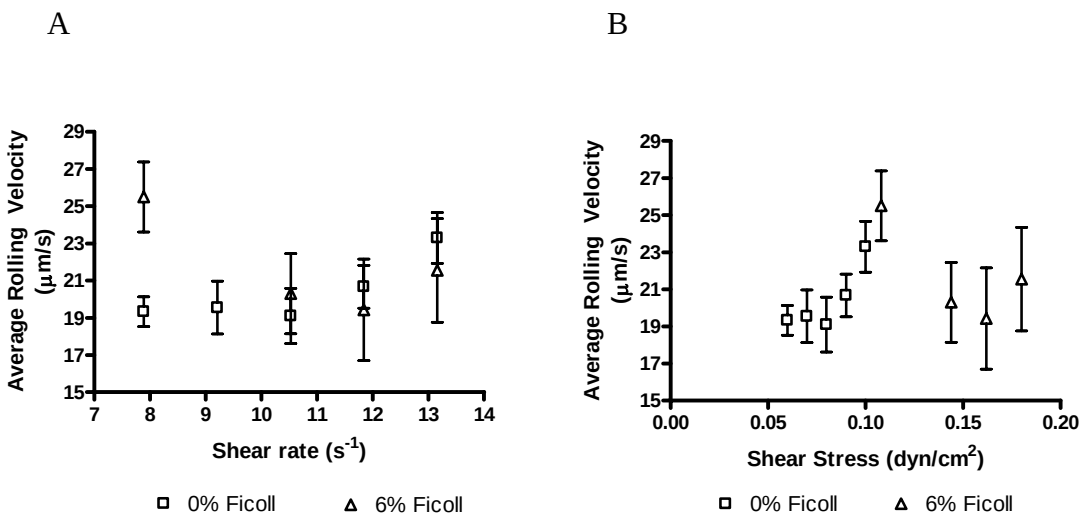

Figure 5.4: Effect of viscosity on the rolling velocities of CHO cells expressing GOF K237V GPIbα interacting with wt vWF-A1. Data represent mean ± SEM and n = 19 to 134 cells.

The addition of 6% Ficoll increases the viscosity at a given shear rate by 1.8 times. Here, the curves for data with and without 6% Ficoll align when plotted versus shear rate (Figure 5.4*A*). In contrast, when rolling velocities are plotted against shear stress, the curves do not align (Figure 5.4*B*). Together, these data suggest that the bonding mechanism may be transport, rather than force, dependent. Because they align with shear rate, this data suggests that transport governs rolling velocity interactions.

5.3 Discussion

Analyzing interactions between GPIbα and vWF molecules shows differences between wt vWF molecules and vWF molecules with mutations causing pt-VWD. The pt-VWD mutation used in these studies was K237V. This mutation shows enhanced binding both in rolling studies [16, 91] and kinetic studies [16] similar to other GOF GPIbα mutations [16, 23, 91-93].

Here we show that CHO cells expressing wt GPIbα interacting with wt vWF-A1 display a biphasic rolling velocity profile. In Figure 5.1, the rolling velocity first decreases, then increases with increasing shear stress. This trend suggests that the CHO cells expressing wt GPIbα are rolling more slowly, and therefore, the bond is lasting for a longer time, a trend indicative of a catch bond. Then, as shear stress is further increased, the rolling velocity increases with increasing shear stress, suggesting that the bond is lasting for increasingly shorter times, a trend indicative of a slip bond. This trend parallels the trend we saw for platelets rolling on wt vWF-A1 (Figure 4.1*A*). As described in Chapter 4, such catch-slip transitions have been previously shown for both selectin interactions [17, 18, 78] and interactions between bacterial FimH and mannose residues on glycoproteins [72, 87]. Although these trends are the same, the transition force is lower for CHO cell interactions compared to platelet interactions on wt vWF-A1 (Figure 5.1 and 4.1 and Table 5.1). A possible reason for this result may be that by isolating the GPIbα receptor and expressing it on CHO cells, the mechanics of binding could be slightly altered resulting in a decreased catch-slip transition shear stress. Alternatively, these data could mean that although wt GPIbα and vWF have similar binding characteristics in clinical tests [8], there may be some differences in the mechanisms at the bond level when comparing isolated wt GPIbα and GPIbα bearing platelets.

To further study the role of GPIbα in GPIbα-vWF interactions, we studied the interactions between CHO cells expressing GOF K237V GPIbα rolling on wt vWF-A1. Here we show in Figure 5.2 that the catch bond at the lowest shear stresses seen for wt-wt interactions (Figure 5.1) is lost resulting in a pure slip bond for these rolling interactions.

These results also parallel the results seen for wt GPIbα (platelets) rolling on GOF vWF-A1 (Figure 4.1*A*). Although the two diseases associated with either a mutation in GPIbα or a mutation in vWF are distinct, they result in a similar clinical diagnosis [8]. It is therefore reasonable to expect the bonding mechanisms underlying each distinct mutation to be similar as is seen in our data. Therefore, these data using CHO cells expressing wt or GOF GPIbα suggest a mechanism for pt-VWD aggregate formation. Loss of the catch bond could result in longer bond lifetimes for GOF mutants at shear stresses where wt molecules would be in the catch bond region. Because lifetimes are increased, bonds last longer allowing aggregates to form.

To further investigate these interactions, and in particular bond lifetimes, the rolling interactions data was extended to determine the mean stop time for wt-wt and GOF-wt interactions. Our results show distinct mean stop time patterns for each wt and GOF mutant GPIbα (Figure 5.3). Here we show that the mean stop time for CHO cells expressing wt GPIbα interacting with wt vWF-A1 first increases, then decreases with increasing shear stress (Figure 5.3, open squares). This data mirrors the rolling velocity data for wt-wt interactions seen in Figure 5.1. While rolling velocity is decreasing (Figure 5.1), the mean stop time is increasing (Figure 5.3). After the catch-slip transition the opposite is observed, where rolling velocity increases (Figure 5.1), while mean stop time decreases (Figure 5.3). Further, we observe that the mean stop time for CHO cells expressing GOF K237V GPIbα interacting with wt vWF-A1 decreases with increasing shear stress (Figure 5.3, open triangles). Again, the mean stop time data is consistent with the rolling velocity data in that as the rolling velocity is increasing (Figure 5.2), the mean stop time is decreasing (Figure 5.3) indicating that as the shear stress is increased

the bond lifetime is decreasing. The results seen here in Figure 5.3 add evidence that the wt-wt bond is regulated by bond lifetime and hence a force mechanism.

To further investigate the role of force on the bonding mechanism, CHO cells expressing GOF K237V GPIbα interactions with wt vWF-A1 were studied with or without the presence of 6% Ficoll, which increases the shear stress at a given shear rate by 1.8 times. In Figure 5.4, we show that the rolling velocity curves for CHO cells expressing GOF K237V GPIbα interacting with wt vWF-A1 align when plotted against shear rate (Figure 5.4*A*), while the curves do not align when plotted against shear stress (Figure 5.4*B*). The data here for CHO cells expressing GOF K237V GPIbα suggest that there is transport dependence in the bond for these GPIbα mutations. The data in Figures 5.3 and 5.4 suggest that the balance between force and transport are likely important for GOF mutations in GPIbα.

Rolling velocity of CHO cells expressing wt or GOF GPIbα interacting with wt vWF-A1 surfaces was measured at 37^{o}C and 250 frames per second. Differences in the shape of rolling velocity curves were observed. Further the effects of a change in force, by changing the viscosity, were observed for rolling velocities. Mean stop time data showed differences between the different GPIbα molecules and that for wt-wt interactions the mean stop time was biphasic as were rolling velocities.

These observations, over a range of shear stresses, reveal the presence of catch-slip transitions at shear stresses that may reflect changes in GPIbα structure. Further studies reveal the loss of this biphasic bonding behavior for CHO cells expressing GOF K237V GPIbα interacting with wt vWF-A1. Additional studies will lead to a greater understanding of how naturally occurring mutations in GPIbα result in pt-VWD. The

data shown here provides details of the GPIbα-vWF tether bond and show differences that exist between different wt and GOF GPIbα molecules. Determination of the biomechanical and kinetic functions of wt and mutant molecules will help elucidate the physiological mechanisms inherent in interactions between GPIbα and vWF. This analysis may lead to a better understanding of pt-VWD bleeding disorders and how they differ in bonding behavior from wt interactions.

CHAPTER 6: CONCLUSIONS

6.1 Summary

In this thesis project the bonding interactions under fluid shear stress between GPIbα and vWF molecules in their wt and disease causing mutant forms were studied. We examined the rolling and tethering interactions between GPIbα and vWF molecules to determine the mechanisms underlying interactions at the bond level between these two molecules. In Chapter 4 platelet interactions with wt and mutant vWF were studied.

In Chapter 4, we studied the bond mechanics when VWD mutations were present. For these studies, one type 2B mutation (GOF R687E) and one type 2M (LOF G561S) vWF mutation were selected. First, we studied the interactions for platelets and various wt vWF molecules and show that all wt-wt interactions have biphasic rolling velocity curves indicating catch-slip transitions are present for each wt molecule, which is similar to data we and our colleagues presented previously [5]. Further, wt molecules were compared with vWF molecules bearing type 2B VWD and type 2M VWD mutations. Rolling velocities for platelets on LOF G561S vWF-A1 retained the catch-slip transition, while rolling velocities for platelets on GOF R687E vWF-A1 displayed only slip bonding behavior.

To further study the mechanism underlying these interactions, the rolling interactions were analyzed to obtain mean stop time. In comparing mean stop time data for wt vWF-A1, LOF G561S vWF-A1, and GOF R687E vWF-A1 we saw that all three vWF molecules had a biphasic relationship with increasing shear stress. Further, the

maximum stop time was shifted to a lower shear stress for the GOF vWF-A1 mutant and to a higher shear stress for the LOF vWF-A1 mutant when compared to wt vWF-A1. When compared with data presented by Auton et al. [86], this data indicates that the mutations in the vWF-A1 domain likely affect the stability of the vWF-A1 domain and subsequently its ability to bind to platelet GPIbα. By being less stable at a lower shear stress compared to wt vWF-A1 molecules (more susceptible to force compared to wt vWF-A1 at its normal transition shear stress), it is likely that GOF vWF-A1 molecules become conformationally active at these low shear stresses and are able to participate in the enhanced binding that is characteristic of type 2B VWD. By becoming more stabilized at higher shear stresses compared to wt vWF-A1 molecules, LOF vWF-A1 molecules likely become conformationally active at shear stresses where they are not able to bind platelets effectively because there are a decreased number of successful interactions at these higher shear stresses. Together these bonding observations combine to provide a possible explanation of the decreased binding that is characteristic of type 2M VWD.

To further study the bonding behavior of the GPIbα-vWF tether bond we show that the mean stop and go times for platelet interactions with wt vWF-A1 molecules differ greatly. Together mean stop and go time data for platelets interacting with wt vWF-A1 suggest that the bond lifetime regulates wt-wt interactions subjected to fluid shear stress, which is consistent both with data presented here as well as data previously presented [5]. Further, the mean go time is constant compared to the mean stop time, suggesting the time spent by the cell moving forward would be unaffected by changes in fluid shear stress when compared to changes in the time the cell spends stopped. Because

the mean go time does not directly measure on rate and instead is an indicator of the total time moving forward, which includes on-rate as well as other forward motions, mean go time data suggests that transport mechanisms may not be as important as force dependent mechanisms. However, mean stop time data suggests platelet interactions with wt vWF-A1 are force dependent.

To gain a better understanding of the role of force for the GPIbα-vWF tether bond, the effect of increasing medium viscosity was studied for rolling velocity and mean stop time of platelets interacting with wt vWF-A1. The resulting data shows that when the viscosity of the platelet suspension buffer is increased 1.8 times, the data aligns when plotted with respect to shear stress, but not when plotted with respect to shear rate. These results indicate that both rolling interactions (both here and in [5]) and mean stop times for platelets and wt vWF-A1 interactions are force, rather than transport dependent.

In addition, the bond life times were measured as kinetic dissociation or off-rates for GPIbα-vWF interactions. Here we show that interactions of platelets with both wt vWF-A1 and LOF G561S vWF-A1 have a biphasic off-rate profile with the off-rate decreasing with increasing shear stress, then transitioning to the off-rate increasing with increasing shear stress, which is consistent with previous data from us and our colleagues [5, 86]. Because off-rate is a direct measurement of how force affects the bond, these data indicate that force plays an important role in the presence of a catch-slip transition for both wt vWF-A1 and LOF G561S vWF-A1.

Preliminary studies looking at the transport mechanism were conducted by observing first time tethering events to calculate on-rate indicators. Here we see that a similar number of tethers are formed per minute for both wt vWF-A1 and LOF G561S

vWF-A1. However, at the higher shear stresses studied the percent of cells at the surface that are tethering is greater for wt vWF-A1 compared to LOF G561S vWF-A1. Combining these results with those seen for changes in mean stop times and force dependency data, this data adds to the evidence that GPIbα-vWF interactions are force dependent, since the since at lower shear stresses these on-rate related data are similar for wt vWF-A1 and LOF G561S vWF-A1.

Finally, in Chapter 4 we study a third bleeding disorder, TTP, which also results in patient bleeding due to an inactive form of or the absence of ADAMTS-13. Our preliminary data shows decreased bond lifetime in the presence of ADAMTS-13 for platelet interactions with whole vWF indicating that there is increased dissociation when ADAMTS-13 is present. These data suggest that in the absence of ADAMTS-13 the dissociation rate is decreased indicating that the GPIbα-vWF bonds last longer and provide evidence for the observation that when the enzyme is absent, platelet aggregates form preventing normal hemostasis at sites of vascular injury.

In Chapter 5 we studied the bond mechanics for mutations in the GPIbα receptor causing pt-VWD. For these studies the GPIbα GOF K237V mutation was selected. Rolling velocities for wt-wt interactions were biphasic, while rolling velocities for CHO cells expressing GOF K237V GPIbα interacting with wt vWF-A1display monophasic behavior only. Both results are similar to the results seen for platelet interactions with wt vWF-A1 and GOF R687E vWF-A1 and indicate there may be catch-slip bond behavior for wt-wt interactions, while there is only slip bond behavior for GOF mutations in GPIbα.

To further study the mechanism underlying these interactions, the rolling interactions were analyzed to obtain mean stop time. Mean stop times for wt-wt interactions are biphasic, while they are monophasic for CHO cells expressing GOF K237V GPIbα interacting with wt vWF-A1. These data indicate there is a catch-slip transition for wt-wt interactions, while there is only a slip bond for GOF GPIbα-wt interactions. The mean stop time is larger for the GOF mutant at lowest shear stress compared to wt GPIbα, these data suggest a possible explanation of why aggregates form when GOF mutations are present: when the molecule pair comes together the bonds last longer for GPIbα molecules carrying a GOF mutation.

To gain a better understanding of the role of force for the GPIbα-vWF tether bond, rolling velocity for CHO cells expressing GOF K237V GPIbα interacting with wt vWF-A1 was measured in the presence or absence of increased viscosity medium. When the data for each condition (with or without an increase in viscosity) are plotted with respect to each shear stress and shear rate, the data align with shear rate, but not necessarily with shear stress. Because they align with shear rate, this data suggests that transport may govern rolling velocity interactions.

Overall, these data indicate a mechanism by which wt-wt interaction prevent aggregate formation and platelet clearance seen for GOF mutations both on the vWF and the GPIbα molecules. Further, these studies give greater insight into how the bonding mechanisms wt-mutant interactions differ from wt-wt interactions and how they may explain bleeding observations seen in disease states. The data presented in this dissertation suggest mechanisms that offer possible explanations for the bleeding seen in type 2B VWD, type 2M VWD, and pt-VWD, by providing insight into how the binding

between GPIbα and vWF can be increased (type 2B VWD and pt-VWD) or decreased (type 2M VWD).

6.2 Future Work

Future studies will seek to further determine the role of both force and transport in the binding mechanism between GPIbα and vWF. These studies will elucidate the degree to which each type of mechanism is involved in normal hemostasis as well as in cases where VWD mutations and pt-VWD mutations are present. These studies will round out the analysis of disease mutations presented in this dissertation and will include rolling velocities and rolling parameters in the presence and absence of increased viscosity for mutations not studied here (platelets with LOF G561S vWF-A and GOF R687E vWF-A1). Further, mean stop times will be determined for platelet interactions with LOF G561S vWF-A1. Additionally, transient tethering lifetimes for platelet interactions with GOF vWF-A1 and for CHO cells expressing GOF K237V with wt vWF-A1 will be completed to directly measure the off-rate of the GPIbα-vWF tether bond when these GOF mutations are present. To observe the role of on-rate and transport mechanisms, the tethering frequency of all disease mutations will be measured. There are two sources for this type of data. The first will come from rolling interactions using the stop-go model used to determine mean stop times presented in this dissertation. These data will be the number of events per second (frequency) for each stop and go events in rolling interaction data. The second type of data will come from tether rate data that describes the behavior of first time tethering events and is a more direct measure of on-rate behavior. These types of analyses have previously been used to describe selectin

interactions [17, 94]. This set of experiments will provide a more complete the story for force and transport dependence of the GPIbα-vWF tether bond for the diseases studied for this dissertation.

Because GOF mutations causing both type 2B VWD and pt-VWD are thought to cause a similar physiological response (aggregates in the bulk fluid), it is also likely that there are similarities for LOF mutations causing type 2M VWD and Bernard Soulier Syndrome. To study the latter mutations, rolling interactions, transient tethering lifetimes, and tethering frequency data for CHO cells expressing LOF Q232V GPIbα interacting with wt vWF-A1 will be measured and compared to results for platelets interacting with LOF G561S vWF-A1. Combining these studies will provide a fuller picture of the GPIbα-vWF tether bond and the changes that occur when bleeding disorders are present.

REFERENCES

1. Goldman, A.J., R.G. Cox, and H. Brenner, *Slow viscous motion of a sphere parallel to a plane wall - II: Couette flow.* Chem. Eng. Sci., 1967. **22**: p. 653-660.

2. Reininger, A.J., *Function of von Willebrand factor in haemostasis and thrombosis.* Haemophilia, 2008. **14 Suppl 5**: p. 11-26.

3. Sadler, J.E., et al., *Update on the pathophysiology and classification of von Willebrand disease: a report of the Subcommittee on von Willebrand Factor.* J Thromb Haemost, 2006. **4**(10): p. 2103-14.

4. Moake, J.L., *Thrombotic thrombocytopenic purpura: the systemic clumping "plague".* Annu Rev Med, 2002. **53**: p. 75-88.

5. Yago, T., et al., *Platelet glycoprotein Ibalpha forms catch bonds with human WT vWF but not with type 2B von Willebrand disease vWF.* J Clin Invest, 2008. **118**(9): p. 3195-207.

6. Rabinowitz, I., et al., *von Willebrand disease type B: a missense mutation selectively abolishes ristocetin-induced von Willebrand factor binding to platelet glycoprotein Ib.* Proc Natl Acad Sci U S A, 1992. **89**(20): p. 9846-9.

7. Morales, L.D., C. Martin, and M.A. Cruz, *The interaction of von Willebrand factor-A1 domain with collagen: mutation G1324S (type 2M von Willebrand disease) impairs the conformational change in A1 domain induced by collagen.* J Thromb Haemost, 2006. **4**(2): p. 417-25.

8. Dumas, J.J., et al., *Crystal structure of the wild-type von Willebrand factor A1-glycoprotein Ibalpha complex reveals conformation differences with a complex bearing von Willebrand disease mutations.* J Biol Chem, 2004. **279**(22): p. 23327-34.

9. Plow, E.F., M.M. Pesho, and Y. Ma, *Integrin αIIbβ3*, in *Platelets*, A.D. Michelson, Editor. 2007, Academic Press. p. 165-178.

10. Andrews, R.K., J.A. Lopez, and M.C. Berndt, *Molecular mechanisms of platelet adhesion and activation.* Int J Biochem Cell Biol, 1997. **29**(1): p. 91-105.

11. Nichols, W.L., et al., *von Willebrand disease (VWD): evidence-based diagnosis and management guidelines, the National Heart, Lung, and Blood Institute (NHLBI) Expert Panel report (USA).* Haemophilia, 2008. **14**(2): p. 171-232.

12. Matsushita, T. and J.E. Sadler, *Identification of amino acid residues essential for von Willebrand factor binding to platelet glycoprotein Ib. Charged-to-alanine scanning mutagenesis of the A1 domain of human von Willebrand factor.* J Biol Chem, 1995. **270**(22): p. 13406-14.

13. de Romeuf, C., L. Hilbert, and C. Mazurier, *Platelet activation and aggregation induced by recombinant von Willebrand factors reproducing four type 2B von Willebrand disease missense mutations.* Thromb Haemost, 1998. **79**(1): p. 211-6.

14. Franchini, M., M. Montagnana, and G. Lippi, *Clinical, laboratory and therapeutic aspects of platelet-type von Willebrand disease.* Int J Lab Hematol, 2008. **30**(2): p. 91-4.

15. Lopez, J.A., et al., *Bernard-Soulier syndrome.* Blood, 1998. **91**(12): p. 4397-418.

16. Kumar, R.A., et al., *Kinetics of GPIbalpha-vWF-A1 tether bond under flow: effect of GPIbalpha mutations on the association and dissociation rates.* Biophys J, 2003. **85**(6): p. 4099-109.

17. Yago, T., et al., *Catch bonds govern adhesion through L-selectin at threshold shear.* J Cell Biol, 2004. **166**(6): p. 913-23.

18. Marshall, B.T., et al., *Direct observation of catch bonds involving cell-adhesion molecules.* Nature, 2003. **423**(6936): p. 190-3.

19. Smith, M.J., E.L. Berg, and M.B. Lawrence, *A direct comparison of selectin-mediated transient, adhesive events using high temporal resolution.* Biophys J, 1999. **77**(6): p. 3371-83.

20. Savage, B., F. Almus-Jacobs, and Z.M. Ruggeri, *Specific synergy of multiple substrate-receptor interactions in platelet thrombus formation under flow.* Cell, 1998. **94**(5): p. 657-66.

21. Doggett, T.A., et al., *Selectin-like kinetics and biomechanics promote rapid platelet adhesion in flow: the GPIb(alpha)-vWF tether bond.* Biophys J, 2002. **83**(1): p. 194-205.

22. Miura, S., et al., *Interaction of von Willebrand factor domain A1 with platelet glycoprotein Ibalpha-(1-289). Slow intrinsic binding kinetics mediate rapid platelet adhesion.* J Biol Chem, 2000. **275**(11): p. 7539-46.

23. Doggett, T.A., et al., *Alterations in the intrinsic properties of the GPIbalpha-VWF tether bond define the kinetics of the platelet-type von Willebrand disease mutation, Gly233Val.* Blood, 2003. **102**(1): p. 152-60.

24. Ruggeri, Z.M., *Structure and function of von Willebrand factor.* Thromb Haemost, 1999. **82**(2): p. 576-84.

25. Siedlecki, C.A., et al., *Shear-dependent changes in the three-dimensional structure of human von Willebrand factor.* Blood, 1996. **88**(8): p. 2939-50.

26. Ramasubramanian, A., *Effects of Unusually Large Multimers of vWF on Platelet-VWF Interactions*, in *Characterization of platelet Glycoprotein Ib-IX-V-vob Willebrand Factor Interaction under Shear Conditions*. 2004: Houston, TX. p. 83-103.

27. Huizinga, E.G., et al., *Structures of glycoprotein Ibalpha and its complex with von Willebrand factor A1 domain.* Science, 2002. **297**(5584): p. 1176-9.

28. Li, F., et al., *Shear stress-induced binding of large and unusually large von Willebrand factor to human platelet glycoprotein Ibalpha.* Ann Biomed Eng, 2004. **32**(7): p. 961-9.

29. Blann, A.D., *Plasma von Willebrand factor, thrombosis, and the endothelium: the first 30 years.* Thromb Haemost, 2006. **95**(1): p. 49-55.

30. Titani, K., et al., *Amino acid sequence of human von Willebrand factor.* Biochemistry, 1986. **25**(11): p. 3171-84.

31. De Marco, L., et al., *Interaction of asialo von Willebrand factor with glycoprotein Ib induces fibrinogen binding to the glycoprotein IIb/IIIa complex and mediates platelet aggregation.* J Clin Invest, 1985. **75**(4): p. 1198-203.

32. Schulte am Esch, J., 2nd, et al., *Impact of O-linked glycosylation of the VWF-A1-domain flanking regions on platelet interaction.* Br J Haematol, 2005. **128**(1): p. 82-90.

33. Foster, P.A., et al., *A major factor VIII binding domain resides within the amino-terminal 272 amino acid residues of von Willebrand factor.* J Biol Chem, 1987. **262**(18): p. 8443-6.

34. Hoylaerts, M.F., et al., *von Willebrand factor binds to native collagen VI primarily via its A1 domain.* Biochem J, 1997. **324 (Pt 1)**: p. 185-91.

35. Bonnefoy, A., et al., *von Willebrand factor A1 domain can adequately substitute for A3 domain in recruitment of flowing platelets to collagen.* J Thromb Haemost, 2006. **4**(10): p. 2151-61.

36. Fujimura, Y., et al., *A heparin-binding domain of human von Willebrand factor. Characterization and localization to a tryptic fragment extending from amino acid residue Val-449 to Lys-728.* J Biol Chem, 1987. **262**(4): p. 1734-9.

37. Matsui, T. and J. Hamako, *Structure and function of snake venom toxins interacting with human von Willebrand factor.* Toxicon, 2005. **45**(8): p. 1075-87.

38. Cruz, M.A., et al., *Interaction of the von Willebrand factor (vWF) with collagen. Localization of the primary collagen-binding site by analysis of recombinant vWF a domain polypeptides.* J Biol Chem, 1995. **270**(18): p. 10822-7.

39. Emsley, J., et al., *Crystal Structure of the von Willebrand Factor A1 Domain and Implications for the Binding of Platelet Glycoprotein Ib.* J Biol Chem, 1998. **273**(17): p. 10396-10401.

40. Thomas, K.B., E.P. Tune, and S.C. Choong, *Parallel determination of von Willebrand factor--Ristocetin and Botrocetin cofactors.* Thromb Res, 1994. **75**(4): p. 401-8.

41. Huizinga, E.G., et al., *Crystal structure of the A3 domain of human von Willebrand factor: implications for collagen binding.* Structure, 1997. **5**(9): p. 1147-56.

42. Celikel, R., et al., *Crystal structure of the von Willebrand factor A1 domain in complex with the function blocking NMC-4 Fab.* Nat Struct Biol, 1998. **5**(3): p. 189-94.

43. Ward, C.M. and M.C. Berndt, *von Willebrand Factor and Platelet Adhesion*, in *Platelets, Thrombosis, and the Vessel Wall*, M.C. Berndt, Editor. 2000, harwood academic publishers. p. 41-64.

44. Lopez, J.A., *The platelet glycoprotein Ib-IX complex.* Blood Coagul Fibrinolysis, 1994. **5**(1): p. 97-119.

45. Berndt, M.C., et al., *The vascular biology of the glycoprotein Ib-IX-V complex.* Thromb Haemost, 2001. **86**(1): p. 178-88.

46. Coller, B.S., et al., *Studies with a murine monoclonal antibody that abolishes ristocetin-induced binding of von Willebrand factor to platelets: additional evidence in support of GPIb as a platelet receptor for von Willebrand factor.* Blood, 1983. **61**(1): p. 99-110.

47. Nurden, A.T. and J.P. Caen, *Specific roles for platelet surface glycoproteins in platelet function.* Nature, 1975. **255**(5511): p. 720-2.

48. Simon, D.I., et al., *Platelet glycoprotein ibalpha is a counterreceptor for the leukocyte integrin Mac-1 (CD11b/CD18).* J Exp Med, 2000. **192**(2): p. 193-204.

49. Okumura, T. and G.A. Jamieson, *Platelet glycocalicin: a single receptor for platelet aggregation induced by thrombin or ristocetin.* Thromb Res, 1976. **8**(5): p. 701-6.

50. Romo, G.M., et al., *The glycoprotein Ib-IX-V complex is a platelet counterreceptor for P-selectin.* J Exp Med, 1999. **190**(6): p. 803-14.

51. Fox, J.E., L.P. Aggerbeck, and M.C. Berndt, *Structure of the glycoprotein Ib.IX complex from platelet membranes.* J Biol Chem, 1988. **263**(10): p. 4882-90.

52. Andrews, R.K. and J.E. Fox, *Identification of a region in the cytoplasmic domain of the platelet membrane glycoprotein Ib-IX complex that binds to purified actin-binding protein.* J Biol Chem, 1992. **267**(26): p. 18605-11.

53. Canobbio, I., C. Balduini, and M. Torti, *Signalling through the platelet glycoprotein Ib-V-IX complex.* Cell Signal, 2004. **16**(12): p. 1329-44.

54. Schade, A.J., et al., *Cytoplasmic truncation of glycoprotein Ib alpha weakens its interaction with von Willebrand factor and impairs cell adhesion.* Biochemistry, 2003. **42**(7): p. 2245-51.

55. Uff, S., et al., *Crystal structure of the platelet glycoprotein Ib(alpha) N-terminal domain reveals an unmasking mechanism for receptor activation.* J Biol Chem, 2002. **277**(38): p. 35657-63.

56. Dong, J.F., C.Q. Li, and J.A. Lopez, *Tyrosine sulfation of the glycoprotein Ib-IX complex: identification of sulfated residues and effect on ligand binding.* Biochemistry, 1994. **33**(46): p. 13946-53.

57. Dong, J., et al., *Tyrosine sulfation of glycoprotein I(b)alpha. Role of electrostatic interactions in von Willebrand factor binding.* J Biol Chem, 2001. **276**(20): p. 16690-4.

58. Marchese, P., et al., *Identification of three tyrosine residues of glycoprotein Ib alpha with distinct roles in von Willebrand factor and alpha-thrombin binding.* J Biol Chem, 1995. **270**(16): p. 9571-8.

59. Ward, C.M., et al., *Mocarhagin, a novel cobra venom metalloproteinase, cleaves the platelet von Willebrand factor receptor glycoprotein Ibalpha. Identification of the sulfated tyrosine/anionic sequence Tyr-276-Glu-282 of glycoprotein Ibalpha as a binding site for von Willebrand factor and alpha-thrombin.* Biochemistry, 1996. **35**(15): p. 4929-38.

60. Tait, A.S., et al., *Site-directed mutagenesis of platelet glycoprotein Ib alpha demonstrating residues involved in the sulfation of tyrosines 276, 278, and 279.* Blood, 2002. **99**(12): p. 4422-7.

61. Tsai, H.M., Sussman, II, and R.L. Nagel, *Shear stress enhances the proteolysis of von Willebrand factor in normal plasma.* Blood, 1994. **83**(8): p. 2171-9.

62. Schneider, S.W., et al., *Shear-induced unfolding triggers adhesion of von Willebrand factor fibers.* Proc Natl Acad Sci U S A, 2007. **104**(19): p. 7899-903.

63. Alexander-Katz, A., et al., *Shear-flow-induced unfolding of polymeric globules.* Phys Rev Lett, 2006. **97**(13): p. 138101.

64. Crawley, J.T., D.E.G. R, and B.M. Luken, *Circulating ADAMTS-13-von Willebrand factor complexes: an enzyme on demand.* J Thromb Haemost, 2009. **7**(12): p. 2085-7.

65. Sadler, J.E., *Von Willebrand factor, ADAMTS13, and thrombotic thrombocytopenic purpura.* Blood, 2008. **112**(1): p. 11-8.

66. Finger, E.B., et al., *Adhesion through L-selectin requires a threshold hydrodynamic shear.* Nature, 1996. **379**(6562): p. 266-9.

67. Lawrence, M.B., et al., *Threshold levels of fluid shear promote leukocyte adhesion through selectins (CD62L,P,E).* J Cell Biol, 1997. **136**(3): p. 717-27.

68. Lou, J., et al., *Flow-enhanced adhesion regulated by a selectin interdomain hinge.* J Cell Biol, 2006. **174**(7): p. 1107-17.

69. Klopocki, A.G., et al., *Replacing a lectin domain residue in L-selectin enhances binding to P-selectin glycoprotein ligand-1 but not to 6-sulfo-sialyl Lewis x.* J Biol Chem, 2008. **283**(17): p. 11493-500.

70. Savage, B., E. Saldivar, and Z.M. Ruggeri, *Initiation of platelet adhesion by arrest onto fibrinogen or translocation on von Willebrand factor.* Cell, 1996. **84**(2): p. 289-97.

71. Thomas, W.E., et al., *Bacterial adhesion to target cells enhanced by shear force.* Cell, 2002. **109**(7): p. 913-23.

72. Thomas, W.E., et al., *Shear-dependent 'stick-and-roll' adhesion of type 1 fimbriated Escherichia coli.* Mol Microbiol, 2004. **53**(5): p. 1545-57.

73. Chang, K.C. and D.A. Hammer, *The forward rate of binding of surface-tethered reactants: effect of relative motion between two surfaces.* Biophys J, 1999. **76**(3): p. 1280-92.

74. Chen, S. and T.A. Springer, *Selectin receptor-ligand bonds: Formation limited by shear rate and dissociation governed by the Bell model.* Proc Natl Acad Sci U S A, 2001. **98**(3): p. 950-5.

75. Dembo, M., et al., *The reaction-limited kinetics of membrane-to-surface adhesion and detachment.* Proc R Soc Lond B Biol Sci, 1988. **234**(1274): p. 55-83.

76. Evans, E., et al., *Chemically distinct transition states govern rapid dissociation of single L-selectin bonds under force.* Proc Natl Acad Sci U S A, 2001. **98**(7): p. 3784-9.

77. Zhao, Y., S. Chien, and S. Weinbaum, *Dynamic contact forces on leukocyte microvilli and their penetration of the endothelial glycocalyx.* Biophys J, 2001. **80**(3): p. 1124-40.

78. Sarangapani, K.K., et al., *Low force decelerates L-selectin dissociation from P-selectin glycoprotein ligand-1 and endoglycan.* J Biol Chem, 2004. **279**(3): p. 2291-8.

79. Isberg, R.R. and P. Barnes, *Dancing with the host; flow-dependent bacterial adhesion.* Cell, 2002. **110**(1): p. 1-4.

80. Chigaev, A., et al., *FRET detection of cellular alpha4-integrin conformational activation.* Biophys J, 2003. **85**(6): p. 3951-62.

81. Cruz, M.A., et al., *Mapping the glycoprotein Ib-binding site in the von willebrand factor A1 domain.* J Biol Chem, 2000. **275**(25): p. 19098-105.

82. Auton, M., M.A. Cruz, and J. Moake, *Conformational stability and domain unfolding of the von Willebrand factor a domains.* J Mol Biol, 2007. **366**(3): p. 986-1000.

83. Lopez, J.A., et al., *Glycoprotein (GP) Ib beta is the critical subunit linking GP Ib alpha and GP IX in the GP Ib-IX complex. Analysis of partial complexes.* J Biol Chem, 1994. **269**(38): p. 23716-21.

84. Alon, R., et al., *The kinetics of L-selectin tethers and the mechanics of selectin-mediated rolling.* J Cell Biol, 1997. **138**(5): p. 1169-80.

85. Chen, S., et al., *Rolling and transient tethering of leukocytes on antibodies reveal specializations of selectins.* Proc Natl Acad Sci U S A, 1997. **94**(7): p. 3172-7.

86. Auton, M., et al., *Changes in thermodynamic stability of von Willebrand factor differentially affect the force-dependent binding to platelet GPIbalpha.* Biophys J, 2009. **97**(2): p. 618-27.

87. Nilsson, L.M., et al., *Catch bond-mediated adhesion without a shear threshold: trimannose versus monomannose interactions with the FimH adhesin of Escherichia coli.* J Biol Chem, 2006. **281**(24): p. 16656-63.

88. Miller, J.L., *Platelet-type von Willebrand disease.* Thromb Haemost, 1996. **75**(6): p. 865-9.

89. Miller, J.L., et al., *Mutation in the gene encoding the alpha chain of platelet glycoprotein Ib in platelet-type von Willebrand disease.* Proc Natl Acad Sci U S A, 1991. **88**(11): p. 4761-5.

90. Russell, S.D. and G.J. Roth, *Pseudo-von Willebrand disease: a mutation in the platelet glycoprotein Ib alpha gene associated with a hyperactive surface receptor.* Blood, 1993. **81**(7): p. 1787-91.

91. Dong, J.F., et al., *Novel gain-of-function mutations of platelet glycopreotein Iba by valine mutagenesis in the Cys209-Cys248 disulfide loop.* J Biol Chem, 2000. **275**: p. 27663-27670.

92. Tait, A.S., et al., *Phenotype changes resulting in high-affinity binding of von Willebrand factor to recombinant glycoprotein Ib-IX: analysis of the platelet-type von Willebrand disease mutations.* Blood, 2001. **98**(6): p. 1812-8.

93. Arya, M., et al., *Dynamic force spectroscopy of glycoprotein Ib-IX and von Willebrand factor.* Biophys J, 2005. **88**(6): p. 4391-401.

94. Yago, T., et al., *Transport governs flow-enhanced cell tethering through L-selectin at threshold shear.* Biophys J, 2007. **92**(1): p. 330-42.